HHS Public Access

Author manuscript

Cell. Author manuscript; available in PMC 2024 November 22.

Published in final edited form as:

Cell. 2023 November 22; 186(24): 5375–5393.e25. doi:10.1016/j.cell.2023.10.019.

S. aureus drives itch and scratch-induced skin damage through a V8 protease-PAR1 axis

Liwen Deng[1], **Flavia Costa**[2,10], **Kimbria J. Blake**[1,10], **Samantha Choi**[1], **Arundhasa Chandrabalan**[3], **Muhammad Saad Yousuf**[4], **Stephanie Shiers**[4], **Daniel Dubreuil**[5], **Daniela Vega-Mendoza**[6], **Corinne Rolland**[7], **Celine Deraison**[7], **Tiphaine Voisin**[1], **Michelle D. Bagood**[8], **Lucia Wesemann**[1], **Abigail M Frey**[1], **Joseph S. Palumbo**[9], **Brian J. Wainger**[5], **Richard L. Gallo**[8], **Juan-Manuel Leyva-Castillo**[6], **Nathalie Vergnolle**[7], **Theodore J. Price**[4], **Rithwik Ramachandran**[3], **Alexander R. Horswill**[2], **Isaac M. Chiu**[1,11]

[1]Department of Immunology, Harvard Medical School, Boston, MA 02215, USA

[2]Department of Immunology and Microbiology, University of Colorado Anschutz Medical Campus, Aurora, CO 80045, USA

[3]Department of Physiology and Pharmacology, University of Western Ontario, London, Ontario N6A 5C1, CA

[4]Department of Neuroscience and Center for Advanced Pain Studies, University of Texas at Dallas, Richardson, TX 75080, USA

[5]Departments of Neurology and Anesthesia, Critical Care and Pain Medicine, Massachusetts General Hospital, Boston, MA 02114, USA

[6]Division of Immunology, Boston Children's Hospital and Harvard Medical School, Boston, MA 02115, USA

[7]IRSD, Université de Toulouse, INSERM, INRAe, ENVT, Université Toulouse III-Paul Sabatier (UPS), Toulouse, France

[8]Department of Dermatology, University of California San Diego, La Jolla, CA 92093

[9]Cancer and Blood Diseases Institute, Cincinnati Children's Hospital Medical Center and the University of Cincinnati College of Medicine, Cincinnati, Ohio, USA

Correspondence: Isaac_chiu@hms.harvard.edu, Isaac Chiu, Harvard Medical School, Department of Immunology, 77 Avenue Louis Pasteur, Boston, MA 02115.

[11]Lead contact

AUTHOR CONTRIBUTIONS

Conceptualization, L.D, F.C., K.J.B., A.R.H., I.M.C.; Methodology, L.D., F.C., K.J.B., S.C., T.V., A.R.H., I.M.C.; Validation, L.D., F.C., K.J.B., S.C.; Formal analysis, L.D., F.C., K.J.B., S.C., N.V, J.M.L.-C.; Investigation, L.D., F.C., K.J.B., S.C., M.S.Y., S.S., A.C., D.D., D.V.-M, T.V., L.W., M.B., C.R., C.D., A.F., J.M.L.-C.; Resources, J.S.P., B.W., T.J.P., R.R., A.R.H., I.M.C.; Project administration, I.M.C.; Funding acquisition, I.M.C. and A.R.H; Visualization, L.D. and I.M.C.; Supervision, B.W., T.J.P., R.R., A.R.H., R.G., I.M.C.; Writing—original draft, L.D., and I.M.C.; Writing—review and editing, L.D., I.M.C. and all authors.

DECLARATION OF INTERESTS

I.M.C. serves on SAB of GSK Pharmaceuticals. Provisional patent application Serial No. 63/438,668, of which some coauthors are inventors, was filed based on these findings.

[10]These authors contributed equally

SUMMARY

Itch is an unpleasant sensation that evokes a desire to scratch. The skin barrier is constantly exposed to microbes and their products. However, the role of microbes in itch generation is unknown. Here we show that *Staphylococcus aureus*, a bacterial pathogen associated with itchy skin diseases, directly activates pruriceptor sensory neurons to drive itch. Epicutaneous *S. aureus* exposure causes robust itch and scratch-induced damage. By testing multiple isogenic bacterial mutants for virulence factors, we identify the *S. aureus* serine protease V8 as a critical mediator in evoking spontaneous itch and alloknesis. V8 cleaves proteinase-activated receptor 1 (PAR1) on mouse and human sensory neurons. Targeting PAR1 through genetic deficiency, siRNA knockdown, or pharmacological blockade decreases itch and skin damage caused by V8 and *S. aureus* exposure. Thus, we identify a mechanism of action for a pruritogenic bacterial factor and demonstrate the potential of inhibiting V8-PAR1 signaling to treat itch.

Graphical Abstract

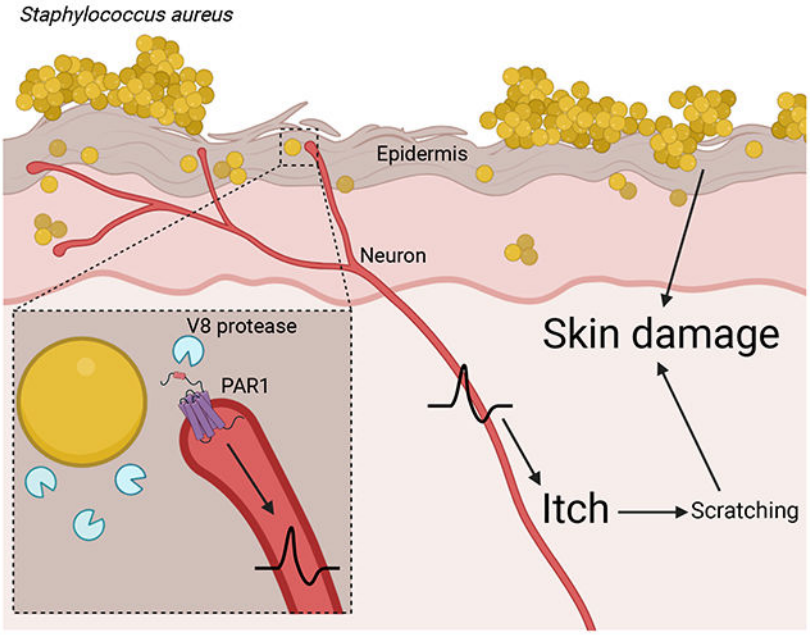

IN BRIEF

Itch evokes a desire to scratch, but the link between microbes and itch was unclear. *Staphylococcus aureus*, a bacterial pathogen, secretes a protease V8 which activates PAR1 expressed on neurons to drive itch and skin damage.

INTRODUCTION

The skin is one of the most exposed barrier sites of the body, susceptible to both injury and pathogen invasion. It is innervated by dorsal root ganglia (DRG) sensory neurons which detect mechanical, thermal, and chemical stimuli, including noxious signals that cause itch

or pain. Pruriceptors are sensory neurons that mediate itch and a desire to scratch[1–3]. Microbes that colonize the skin play key roles in tissue homeostasis and physiology. However, a causative role for microbes in driving itch was unknown. We hypothesized that pruriceptors maybe activated following exposure to specific microbes, resulting in itch that drives skin damage.

Staphylococcus aureus is opportunistic bacterial pathogen and leading cause of human bacterial infections. Atopic dermatitis (AD) is a skin disease characterized by itchy, eczematous lesions. 90% of AD lesions are colonized with *S. aureus*, which is thought to be a trigger of inflammation[4–7]. *S. aureus* is also a leading cause of impetigo, a contagious skin infection characterized by itchy lesions[8]. Despite its association with these pruritic conditions, the contribution *of S. aureus* to itch is unclear. *S. aureus* encodes several virulence factors that promote colonization and tissue invasion, including α-hemolysin (Hla), phenol soluble modulins (PSMs), and proteases[9,10]. Methicillin-resistant *S. aureus* (MRSA) continues to spread, necessitating an improved understanding of bacterial pathogenesis and host responses to this pathogen[4,11]. We previously found that nociceptors detect *S. aureus* and its toxins to produce pain during subcutaneous infections[12–14]. Pruriceptor nerve endings are mainly found in the epidermis, unlike nociceptors, which innervate both skin and deeper tissues[1].

Itch provokes a desire to scratch, a behavioral reflex that could exacerbate skin damage. The importance of the itch-scratch cycle in skin pathology and negative impact on patient quality of life is well known for conditions including AD[15], prurigo nodularis[16], and psoriasis[17]. Scratching produces pain, which can temporarily suppress itch through spinal circuitry[18,19]. Mechanical damage caused by scratching disrupts the skin barrier and can amplify inflammation. Therefore, understanding the triggers and factors that cause itch is critical for treatment of skin diseases.

Here we find that *S. aureus* epicutaneous exposure induces robust itch and scratch-induced damage, which is mediated by the V8 protease. Pruriceptors are activated by V8 protease through PAR1. Targeting PAR1 abrogates itch, leading to improved skin pathology. Our findings uncover a role for bacterial proteases in itch and PAR1 as a candidate for therapeutic development.

RESULTS

Epicutaneous *S. aureus* exposure induces itch and alloknesis

To investigate how *S. aureus* impacts itch, we adapted a murine model of epicutaneous exposure relevant to AD[20–23]. In this model, *S. aureus* is applied topically to depilated back skin under gauze, and mice wrapped with occlusive Tegaderm tape during bacterial exposure, resulting in epidermal breakdown at the inoculation site. At the experimental endpoint, tape and gauze are removed for inflammation and itch analysis (Fig. 1A, Fig. S1A).

We utilized USA300/LAC MRSA strain, which represents the leading cause of community-associated MRSA[24]. Female and male mice were treated with MRSA, and inflammation

scored at 5-days post-exposure. MRSA induced significant exposure-site dermatitis, quantified as a sum of edema, skin scale, erythema, thickness in both sexes (Fig. 1B). Histology showed hyperkeratosis, spongiosis, and inflammatory infiltrates (Fig. S1B). *S. aureus*-exposed mice showed higher transepidermal water-loss (TEWL) than controls, indicating disruption of skin barrier function (Fig. S1C).

We next investigated the role of *S. aureus* in itch. Spontaneous itch behaviors were assessed by placing mice in an infrared behavior observation box (iBOB) to record animals' activity over 90 min (Fig. 1C). Videos watched by blinded observers quantified scratching bouts (Supplemental video 1). Control mice produced minimal scratching while male and female animals treated with *S. aureus* exhibited significantly increased scratching behaviors (Fig. 1D). While dermatitis was observed by day 3, significantly increased scratching behaviors occurred by day 5 after *S. aureus* application (Fig. S1D–E).

Alloknesis is itch evoked by innocuous mechanical stimuli or touch[1,25]. It is a form of dysesthesia driven by pruriceptor sensitization or spinal cord changes[25,26] and regulated by Merkel cells[27]. Alloknesis can potentiate the itch-scratch cycle in AD patients. In mice, alloknesis is measured by stimulation with a 0.07 g filament that normally does not elicit responses, but induces itch following sensitization[28]. We stimulated mice with this filament 9 times and quantified scratching (Supplemental Video 2). MRSA application induced significant alloknesis compared to PBS-treated controls (Fig. 1E). While prior reports showed sex-dependent differences in itch[29,30], we found no differences in MRSA-induced itch and alloknesis between female and male mice (Fig. 1D–E).

Itch induced scratching exacerbates skin damage

Itch-evoked scratching exacerbates skin damage in AD patients. To quantify damage caused by scratching, *S. aureus* exposed mice were allowed to freely scratch the back for 7-hrs after Tegaderm/gauze removal. Total area of damaged skin was quantified using image analysis. Compared to controls, mice inoculated with MRSA had dramatically increased total damaged skin following scratching, resulting in areas of skin damage beyond bacterial exposure site (Fig. 1F). We confirmed that scratching drives damage by wrapping a cohort of infected mice with bandages after Tegaderm/gauze removal. Wrapped mice prevented from scratching had significantly less skin damage than mice allowed to scratch (Fig. 1G). As a second way to prevent scratching, we trimmed nails of mice after Tegaderm/gauze removal (Fig. S1F). Nail trimming reduces itch/scratch-induced damage in mice[31]. Female and male mice that received nail trims had less skin damage than control mice after 7-hrs of recording (Fig. S1G).

Subcutaneous *S. aureus* infection does not induce itch

S. aureus is also a leading cause of human abscesses due to subcutaneous infections[11,24]. However, dermonecrotic skin infections are often painful but not itchy. We next determined whether *S. aureus* deeper infections caused itch. We infected mice with MRSA by injecting subcutaneously in the back, inducing skin lesions by day 5 (Fig. 1H). Epicutaneous applications were performed in parallel, and itch behaviors measured. While spontaneous itch and alloknesis occurred after epicutaneous MRSA exposure, mice

infected subcutaneously did not show spontaneous itch or alloknesis (Fig. 1I–1J). Therefore, while epicutaneous application causes itch, subcutaneous infection does not, indicating that bacterial localization affects neuronal phenotypes.

MYD88, mast cells and basophils do not mediate *S. aureus* itch

Given that *S. aureus* exposure mediates itch, determining underlying mechanisms could lead to therapies to limit itch-induced skin damage. Previous studies showed that *S. aureus* exposure induces IL-36 release, which activates IL-36R signaling through MYD88 to drive skin inflammation[20]. Using *Myd88*$^{-/-}$ mice, we observed a significant reduction in dermatitis and TEWL after *S. aureus* exposure compared to WT mice (Fig. S2A–B). Bacterial load did not differ (Fig. S2C). However, we did not detect differences in spontaneous itch behaviors or alloknesis in *Myd88*–/− mice compared to controls following *S. aureus* exposure (Fig. S2D–E).

Mast cells are key drivers of itch by releasing pruritogens including histamine, serotonin, and tryptase[32]. We utilized *Kit*$^{W\text{-}sh}$ mice, which lack mast cells, to determine their role in *S. aureus* itch. We found no difference in dermatitis or TEWL between *Kit*$^{W\text{-}sh}$ and WT animals following *S. aureus* application (Fig. S2F–G), but there was an increase in bacterial load in *Kit*$^{W\text{-}sh}$ mice (Fig. S2H). We did not detect differences between WT and *Kit*$^{W\text{-}sh}$ mice in spontaneous itch and alloknesis following MRSA exposure (Fig. S2I–J). Basophils also drive itch in AD by release of leukotrienes, histamine and serotonin[33,34]. To determine whether basophils mediate itch during *S. aureus* exposure, we treated mice with Ba103 antibody to deplete basophils[35] or control IgG (Fig. S2K). Flow cytometry revealed basophil recruitment in mouse skin following *S. aureus* exposure and that Ba103 antibody successfully eliminated basophils (Fig. S2L). After *S. aureus* exposure, we observed no differences in dermatitis, TEWL, bacterial load, spontaneous itch, and alloknesis between mice injected with Ba103 and mice injected with control IgG (Fig. S2M–Q). Taken together, mast cells and basophils are not required for *S. aureus*-induced itch or dermatitis.

IL31RA, IL4RA, and lymphocytes do not mediate *S. aureus* itch

Itch is associated with type 2 inflammation and can be driven by cytokines including IL4, IL13, and IL31[36]. We investigated the role of IL31 in *S. aureus*-mediated itch. IL31 was elevated in skin on day-5 after *S. aureus* exposure (Fig. S3A). We administered siRNA via intrathecal injection[37] to knock down expression of the IL31 receptor, *Il31ra*, in DRG neurons. RT-qPCR analysis of thoracic DRGs confirmed that *Il31ra* siRNA reduced *Il31ra* expression compared to control siRNA injection (Fig. S3B). Mice treated with *Il31ra* siRNA showed no differences in *S. aureus* induced dermatitis, TEWL, bacterial load, spontaneous itch, and alloknesis compared to control siRNA-treated mice (Fig. S3C–G). Pruriceptors also express *IL4ra*, which mediates IL4 and IL13 signaling to drive itch[33]. We exposed *Il4ra*$^{-/-}$ and WT control mice to *S. aureus*. We observed no differences in dermatitis, TEWL, bacterial load, spontaneous itch, and alloknesis between *Il4ra*$^{-/-}$ and control mice (Fig, S3H–L). Therefore, type 2 cytokines likely do not mediate *S. aureus* induced itch.

We next ascertained roles for lymphocytes in itch. *Rag2*$^{-/-}$*Il2gr*$^{-/-}$ mice are deficient in T, B, NK cells and ILCs[38,39]. Following MRSA exposure, we did not observe differences

in dermatitis, TEWL, spontaneous itch, and alloknesis in *Rag2*$^{-/-}$*Il2gr*$^{-/-}$ mice compared to WT controls (Fig. S3M–N, P–Q). We recovered more tissue bacteria load from *Rag2*$^{-/-}$*Il2rg*$^{-/-}$ mice, indicating that lymphocytes affect bacterial clearance (Fig. S3O). Overall, we ruled out a role for MYD88, mast cells, basophils, IL31RA, IL4RA, and lymphocytes in itch (Table S1).

S. aureus localizes near epidermal sensory nerves

Pruriceptive nerve endings are mainly located in epidermis[40]. We hypothesized that bacteria may localize to areas close to nerves during epicutaneous exposure to drive itch. Nav1.8 is a voltage-gated sodium channel expressed in C-fibers including pruriceptors[41,42]. *Nav1.8-Cre* mice were bred with tdTomato reporter mice to label sensory neurons. Mice were topically treated with GFP-expressing MRSA or PBS. Whole mount imaging showed Nav1.8-TdTomato^{+} nerves in dermis and epidermis. Sensory innervation was maintained throughout the thickened dermis and epidermis below the *S. aureus* exposure site. In MRSA-exposed mice, we observed GFP^{+} bacteria localized close to Nav1.8-TdTomato+ sensory nerves in the epidermis (Fig. 2A).

S. aureus Agr is required for itch

Because bacteria were localized close to nerve endings, we hypothesized that secreted factors from *S. aureus* could activate neurons to drive itch. *S. aureus* virulence factors are regulated by its Agr quorum sensing system, including expression of multiple secreted cytolytic toxins and proteases (Fig. 2B)[43]. Mice were exposed to WT MRSA or an Δ*agr* isogenic mutant strain. We observed significant reductions in spontaneous itch and alloknesis in mice exposed to Δ*agr* compared to WT MRSA (Fig. 2C). Δ*agr* strain also induced less dermatitis (Fig. 2D). Fewer bacteria were recovered from skin of Δ*agr* compared to WT MRSA-exposed mice (Fig. S4A). Thus, Agr mediates both itch and inflammation.

Bacterial toxins (Hla, PSMs) do not mediate *S. aureus* itch

Agr controls expression of phenol soluble modulins (PSMs) and α-hemolysin (Hla) (Fig. 2B). We tested requirement of these toxins in itch by inoculating mice with WT MRSA or isogenic strains lacking Hla (Δ*hla*) or PSMs (Δ*psm*α Δ*psm*β Δ*hld*; ΔPsms). Epicutaneous exposure to Δ*hla* or ΔPsms MRSA resulted in similar spontaneous itch and alloknesis as WT MRSA (Fig. 2E). MRSA ΔPsms caused less exposure-site dermatitis than WT MRSA, whereas MRSA Δ*hla* induced similar inflammation as WT MRSA (Fig. 2F). These results are in line with previous reports demonstrating PSMs driving inflammation[20,23]. We observed no differences in bacterial load for WT, Δ*hla*, or ΔPsms MRSA (Fig. S4A). Thus, *S. aureus* toxins are not required for itch. Furthermore, itch and inflammation can be decoupled, given that MRSA ΔPsms induced itch despite absence of dermatitis (Fig. 2E–F).

Proteases are necessary for *S. aureus* itch

Proteases from plants, allergens, and mammals have been shown to cause itch[44,45]. *S. aureus* produces 10 proteases including cysteine, serine, and metalloproteases[46], and these proteases are under Agr control (Fig. 2B). We tested the requirement for *S. aureus* proteases in itch

by inoculating mice with WT MRSA or isogenic mutant lacking genes for all 10 proteases (Δ*aur*Δ*sspAB*Δ*scpA*;*spl*::erm; ΔProtease)[47]. Spontaneous itch behaviors and alloknesis were significantly reduced in mice exposed to Δprotease compared to WT MRSA (Fig. 2G). MRSA Δprotease strain was shown previously to induce less inflammation[48]. We found a similar reduction in dermatitis in animals inoculated with Δprotease compared to WT MRSA (Fig. 2H), and decreased bacterial load (Fig. S4A). Therefore, *S. aureus* proteases are necessary for itch and inflammation.

We next aimed to identify the role of specific *S. aureus* protease(s) in itch. Compared to WT MRSA, treatment with MRSA lacking aureolysin (Δ*aur*) resulted in no difference in dermatitis, while a strain deficient in both staphopain A and staphopain B (Δ*scpA*Δ*sspB*) caused a slight decrease in dermatitis (Fig. S4B). Mice inoculated with Δ*aur* or Δ*scpA*Δ*sspB* had no differences in spontaneous itch, alloknesis, or bacterial load compared to mice treated with WT MRSA (Fig. S4A, C–D). MRSA secretes 6 serine protease-like proteins (Spls). MRSA lacking all serine protease-like proteins SplA-F (*spl*::erm) caused a similar degree of dermatitis, spontaneous itch, and alloknesis as WT MRSA (Fig. S4B–D). These data rule out 9/10 known proteases in itch, narrowing the search to serine protease V8, which is encoded by *sspA* gene[49].

S. aureus V8 protease contributes to itch and skin inflammation

To test the requirement of V8 protease in itch, we generated a *sspA* deletion mutant (Δ*sspA*) that does not disrupt downstream *sspB* gene encoding Staphopain B (Fig. S5A). We also engineered chromosomally complemented strain Δ*sspA*+*sspA* and confirmed loss of V8 protease activity in Δ*sspA* and restoration of protease activity in Δ*sspA*+*sspA* complement (Fig. S5A). Epicutaneous application of Δ*sspA* MRSA resulted in significantly less itch behaviors measured by spontaneous itch and alloknesis compared to WT bacteria (Fig. 3A–B). Itch behaviors were restored in mice exposed to Δ*sspA*+*sspA* strain (Fig. 3A–B). Reduction in scratching resulted in decreased total skin damage in animals exposed to MRSA Δ*sspA* (Fig. 3C). Epicutaneous application of Δ*sspA* MRSA resulted in reduction in dermatitis and lower TEWL measurements, indicating reduced skin barrier damage, compared to mice inoculated with WT or complemented MRSA strains (Fig. 3D, Fig. S5B). We observed no differences between WT and MRSA Δ*sspA* strains in adherence to KERTr keratinocyte cells *in vitro*, suggesting that reduction in itch and inflammation are independent of adherence defects (Fig. S5C). We did observe a decrease in tissue bacterial load in mice infected with Δ*sspA* mutant (Fig. S5D). Therefore, V8 protease is a critical bacterial factor that drives itch. Mutant bacterial strains used and role of bacterial factors on itch and inflammatory parameters are summarized in Table S1.

V8 is upregulated in mouse skin and human AD skin lesions

Having identified V8 protease as a mediator of itch, we next quantified *sspA* transcript at different time points in *S. aureus* exposure model (Fig. 3E). *sspA* transcript increased over time, becoming significantly higher on day 5 compared to day 1 post-exposure (Fig. 3F). By contrast, *psmA1* transcript did not change and we did not detect *hla* transcript from mouse skin samples during MRSA exposure (Fig. 3G–H). The timing of increased *sspA* transcript coincides with when we observed robust induction of itch (Fig. S1E). We next

determined whether *S. aureus* V8 (*sspA*) is expressed in human skin samples relevant to disease. We obtained skin swabs from healthy individuals, non-lesional and lesional skin from AD patients. We observed significantly higher amounts of *sspA* transcript in lesional AD skin samples compared to healthy controls (Fig. 3I).

V8 injection induces itch and skin damage

We next tested whether purified V8 protease causes spontaneous itch or pain behaviors. Following intradermal cheek injections, pruritogens induce mice to scratch with the hind-paw, whereas pain-inducing algogens cause mice to wipe with the forelimb (Fig. 3J)[50,51]. We found that injecting 40U V8 protease induced robust itch and not pain (Fig. 3K–L). As a positive control and comparison, we injected mice with histamine, a pruritogen which produced itch (Fig. 3K–L). By contrast, the TRPV1 ligand capsaicin caused pain behaviors (Fig. 3K–L). V8 protease injection induced itch in a dose-dependent manner (Fig. S5E). Itch likely depends on protease activity, as mice injected with heat-inactivated V8 did not exhibit increased scratching compared to untreated V8 (Fig. S5F). While 40U of V8 protease induced itch specifically, 200U of V8 caused both itch and pain behaviors (Fig. S4G–H).

V8 protease injection was also sufficient to cause alloknesis. Mice injected with vehicle, histamine, or V8, followed by alloknesis measurements (Fig 3M). V8 protease resulted in significantly higher alloknesis at every time point measured up to 1 hr compared to histamine and buffer alone (Fig. 3N), and remained elevated in V8-treated mice at 3 hrs post-injection (Fig. S5I).

We next tested whether V8-induced scratching drives skin damage. Mice were injected intradermally into back skin with PBS or V8. One set of V8-injected mice were allowed to scratch while another group was prevented from scratching by wrapping with bandages (Fig. S5J). At 3- and 6-hrs post-injection, V8 protease-injected mice that could scratch exhibited higher TEWL than PBS-injected controls, indicating skin barrier damage (Fig. S5K–L). In contrast, V8 protease did not induce higher TEWL in animals prevented from scratching compared to PBS-injected controls (Fig. S5K–L).

V8 protease cleaves PAR1

We hypothesized that specific host receptors may mediate neuronal recognition of V8 protease to drive itch. Proteinase-activated receptors (PARs) are G protein-coupled receptors activated by proteolytic cleavage of an extracellular N-terminal domain, leading to exposure of a tethered ligand that induces activation[52,53]. Humans and mice express four PAR family members, with PAR1, PAR2, and PAR4 having intracellular signaling capabilities[54,55]. PARs are expressed in pruriceptive neurons and their activities linked to itch[45].

We employed a luminescence-based PAR cleavage assay[56] to determine whether V8 can proteolytically cleave PARs (Fig. 4A). V8 protease potently cleaved human PAR1 (EC_{50} = 4 Units of activity (U)/mL), but did not cleave PAR2, and had modest activity in cleaving PAR4 (EC_{50} = 219 U/mL) (Fig. 4B). As positive controls, we performed PAR cleavage assays with canonical PAR-ligand proteases thrombin (PAR1, PAR4) or trypsin (PAR2) (Fig. 4C). As a second assay, human embryonic kidney (HEK-293) cells expressing PAR1 tagged N-terminally with mRFP and C-terminally with eYFP were exposed to V8. Microscopy

showed V8 treatment resulting in cleavage and removal of N-terminal mRFP tag. Only cleaved receptor (solely eYFP-positive) was detected at cell membrane after V8 exposure (Fig. S6A).

To map potential V8 cleavage sites in N-terminus of PAR1, we incubated a limiting concentration of V8 protease with C-terminally His_6-tagged ligand of human PAR1 ($hPAR1^{22–102}$) attached to Ni-NTA beads. Mass spectrometry analysis of supernatant identified 10 cleavage sites (Fig. 4D, S6B, Table S2) including sites upstream and downstream of canonical thrombin cleavage site (R^{41}/S^{42}), and several peptide fragments. V8 protease did not cleave at E/D|P, possibly due to steric hindrance documented with other proteases[57]. We tested whether V8 protease cleaves the tethered ligand and disarms PAR1 by monitoring thrombin evoked calcium signaling in HEK cells expressing hPAR1 after exposure to V8. We observed no change in intracellular calcium between cells treated with thrombin alone or pre-treated with 2 U/mL V8 protease and thrombin, indicating that, at a lower concentration, V8 cleaves upstream of the thrombin cleavage site (Fig. S6C). At 20 U/mL, V8 abrogated responses to thrombin, suggesting that V8 can cleave downstream of thrombin site at higher concentrations (Fig. S6D). We further tested whether V8 affected PAR1 activation by the synthetic peptide TFLLR-NH_2, observing no inhibition of TFLLR-NH_2 response with 2 U/mL and 20 U/mL V8 protease (Fig. S6E–F). Intact TFLLR-NH_2 responses suggest that V8 does not cleave at receptor sites involved in tethered ligand binding such as extracellular loops and ligand binding pocket.

PAR1 is expressed by DRG neurons

PAR1 expression and activation has been demonstrated in human and mouse DRG neurons[58,59]. We determined whether PAR1 is expressed in DRG neurons linked to itch. PAR1 is encoded by *F2r* gene[53,60]. We performed RNAscope *in situ* hybridization (ISH) analysis in mouse DRG to visualize *F2r* transcripts along with pan-neuronal marker *Tubb3* (Fig. 4E), finding *F2r* expression in 40% of mouse DRG neurons (Fig. 4F). Analysis of a scRNAseq dataset of mouse neurons[61] showed *F2r* expression in several DRG subsets, including neurons previously linked to itch: NP2 neurons that express *mrgpra3* and *hrh1*[2,32], and peptidergic neurons that express *s1pr3*[62] (Fig. S7A). We also performed RNAScope analysis of *F2R* expression in human DRG samples, observing *F2R* in 35% neurons, in accordance with previous studies[59]. $F2R^+$ neurons were small in diameter (average 53.1 μm) and positive for *TRPV1* and *NPPB*, a marker of pruriceptive neurons[63,64] (Fig. 4G–H). Mining scRNAseq data of human DRG neurons, we detected enrichment of *F2R* in a subset of putative pruriceptors expressing NPPB, IL31RA and GFRA2 (Fig. S7B)[65].

V8 activates mouse and human DRG neurons

Having confirmed that purified V8 protease induces itch and cleaves PAR1, we next tested whether V8 could directly activate sensory neurons. Mouse DRG neurons were loaded with calcium indicator Fura-2, followed by application with vehicle or V8 protease. V8 protease induced DRG neuron calcium influx, including a concentration-dependent increase in the number of responsive neurons and the amplitude of calcium responses to V8 (Fig. S7C–D). We subsequently analyzed neuronal responses to 40 U/mL of V8, an amount that induced itch *in vivo* (Fig. 3) and at mid-dose range (Fig. S7C). At 40 U/mL, V8 protease induced

intracellular calcium responses in ~10% of mouse DRG neurons (Fig. 5B). Neurons were subsequently exposed to pruritogens histamine, chloroquine, or sphingosine-1-phosphate (S1P), followed by capsaicin and KCl to mark ligand-responsive subsets (Fig. 5A). Many V8-responsive cells also responded to pruritogens: V8 activated 25% histamine-responsive, 38% chloroquine-responsive, 25% S1P-responsive neurons; V8 activated 22% capsaicin-responsive neurons (Fig. 5B, S7E).

We previously showed that *S. aureus* Hla and N-formylated peptides can activate DRG neurons to mediate pain[12]. Using calcium imaging, we determined whether V8-responsive neurons responded to Hla or fMLF. Hla induced the highest proportion of DRG neuron responses, followed by V8, then fMLF (Fig. S7F). ~74% V8-responsive neurons responded to Hla, and ~26% V8-responsive neurons to fMLF (Fig. S7F). We next performed intradermal cheek injections with Hla or fMLF. While fMLF did not induce itch or pain, Hla injection induced both itch and pain (Fig. S7G). These data suggest that Hla is capable of inducing itch, though ΔHla mutant MRSA did abrogate itch following *S. aureus* exposure (Fig. 2).

We also tested whether human DRG neurons could respond to V8 with freshly dissociated DRG neurons dissected from organ donors. Human neurons were loaded with the calcium indicator Fluo-4, and intracellular calcium changes measured after treatment with V8 protease and capsaicin (Fig. 5C). 26.5% of human DRG neurons were activated by V8, and 95.5% of V8 responsive cells responded to capsaicin (Fig. 5D). These data show that V8 can induce calcium influx in both mouse and human DRG neurons.

PAR1 mediates V8 induced neuronal activation and itch

To test whether V8 activation of neurons is dependent on PAR1, we performed calcium imaging of DRG neurons from wildtype ($F2r^{+/+}$) or $F2r^{-/-}$ mice. Compared to neurons from wildtype animals, $F2r^{-/-}$ neurons were not responsive to treatment with V8 protease (Fig. 5E). We asked if blocking protease activity or PAR1 signaling reduces neuron responses to V8. Mouse DRG neurons were pre-treated with serine protease inhibitor TLCK[66,67] or PAR1 antagonist Vorapaxar[68] (Fig. 5F). Pre-treatment with TLCK or Vorapaxar eliminated V8-induced calcium influx in neurons (Fig. 5F–G). In contrast, neither Vorapaxar nor TLCK affected responses to capsaicin (Fig. 5F, H). These results demonstrate that PAR1 is required for V8 activation of sensory neurons.

We next tested the requirement of PAR1 for V8-induced itch *in vivo*. We performed intradermal cheek injections with PBS or V8 protease into wildtype (WT) and $F2r^{-/-}$ mice. V8 elicited significantly less scratching in $F2r^{-/-}$ mice than WT mice, and no significant differences between V8 and PBS-treatment in $F2r^{-/-}$ mice (Fig. 6A). To determine whether V8 injection induces immune cell recruitment dependent on *F2r*, we performed flow cytometry to characterize skin immune cells in WT and $F2r^{-/-}$ mice after treatment with PBS or V8 (Fig. S8A). We observed a baseline increase in T cells in $F2r^{-/-}$ mice compared to WT, and increased T cells in WT mice treated with V8 compared to PBS. Macrophages decreased in $F2r^{-/-}$ mice at baseline, and further decreased in mice injected with V8. There were no changes in neutrophils, eosinophils, mast cells, basophils, and dendritic cells (Fig. S8B).

We examined the contribution of other protease-activated receptors in V8-induced itch. DRG neurons express various members of the Mas-related G coupled receptors (MRGPRs) family, including MRGPRA3, MRGPRX1, and MRGPRD, which have been linked to itch[69]. We found that mice lacking the Mrgpr locus (*Mrgpr*$^{-/-}$) showed similar acute itch behaviors following V8 intradermal cheek injection as wild-type mice (Fig. S9A). PAR2, encoded by *F2rl1*, also mediates protease-induced itch responses[45,70]. However, we did not find PAR2 cleavage by V8 (Fig. 4B). *F2rl1*$^{-/-}$ mice also showed similar itch as WT mice when injected with V8 (Fig. S9A).

F2r targeting in DRG neurons inhibits V8 and *S. aureus* itch

We next determined the role of *F2r* in DRG neurons in V8-induced itch using siRNA and conditional knockout approaches. Using intrathecal injections of siRNA to target sensory neurons[37], we injected mice with vehicle, control siRNA, or *F2r* siRNA (Fig. 6B). RT-qPCR of thoracic DRGs confirmed efficient knockdown of *F2r* in animals treated with *F2r* siRNA but not control siRNA (Fig. S9B). We next injected V8 protease intradermally at the upper back of mice to observe spontaneous scratching behaviors. *F2r* siRNA-treated animals had significantly reduced V8-induced itch compared to mice injected with vehicle or control siRNA (Fig. 6B). We next determined if *F2r* knockdown in DRGs inhibits itch during epicutaneous *S. aureus* exposure. Following *F2r* or control siRNA injection, mice were inoculated with WT MRSA or treated with PBS (Fig. 6C). At 5-days post-exposure, we observed no differences in dermatitis, skin barrier damage (TEWL), and tissue bacterial load between control and *F2r* siRNA treated mice (Fig. S9C–E). We observed a significant reduction in spontaneous itch behaviors and alloknesis for mice injected with *F2r* siRNA (Fig. 6D–E). *F2r* knockdown mice also showed less total skin damage caused by scratching (Fig. 6F). Therefore, knockdown of *F2r* expression in DRG neurons leads to inhibition of itch caused by V8 protease and *S. aureus*.

To target *F2r* specifically in sensory neurons, we generated *Trpv1*$^{\Delta F2r}$ conditional knockout mice by crossing *Trpv1*^{cre} with *F2r*$^{fl/fl}$ mice (Fig. 6G). *Trpv1*^{cre} lineage-based analysis has shown that it targets both peptidergic and non-peptidergic C-fibers[71]. *Trpv1*$^{\Delta F2r}$ mice or cre-negative control littermates were treated with PBS or exposed to MRSA. We found no differences in dermatitis, TEWL, and skin bacterial load between the two groups (Fig. S9F–H). Similar to mice injected intrathecally with *F2r* siRNA, *Trpv1*$^{\Delta F2r}$ mice exhibited significantly less spontaneous itch and alloknesis following MRSA exposure compared to control mice (Fig. 6H–I).

PAR1 pharmacological inhibition reduces *S. aureus* itch and skin damage

We next investigated the therapeutic potential of PAR1 blockade in blocking itch and skin pathology. Vorapaxar is an FDA-approved PAR1 antagonist and drug used for reducing the risk of thrombotic cardiovascular events[72]. We found that co-administration of V8 and Vorapaxar resulted in significantly reduced scratching for all doses of Vorapaxar tested (Fig. 7A). We also tested the effect of another PAR1 antagonist, SCH79797, and found that all doses of this drug reduced scratching responses to V8 (Fig. S9I). In contrast, PAR4 antagonist BMS986120 minimally affected V8-induced itch, though it did have anti-pruritic effects at the highest dose (Fig. S9J). SCH79797 has direct antimicrobial effects, whereas

Vorapaxar does not affect bacterial growth[73,74]. Therefore, we focused on Vorapaxar for further tests in mice.

Vorapaxar also significantly reduced V8 protease-induced alloknesis. We found that vorapaxar treatment reduced alloknesis responses up to 3 hours after V8 injection (Fig. 7B–C). Mice injected with V8 protease had higher TEWL measurements in back skin, which could be blocked by Vorapaxar treatment or wrapping with bandages to prevent scratching (Fig. 7D). Therefore, blocking PAR1 reduced itch and scratch-induced skin barrier damage after V8 injection.

We next investigated whether Vorapaxar could treat itch during *S. aureus* epicutaneous exposure. Mice were gavaged daily with Vorapaxar or vehicle control (Fig. 7E). We found that, similar to *F2r* siRNA, Vorapaxar treatment had no effect on dermatitis, TEWL, and bacterial load (Fig. 7F, S9K–M). Vorapaxar significantly reduced spontaneous itch behaviors and alloknesis following epicutaneous *S. aureus* application (Fig. 7G–H). We also recorded less skin damage from scratching for the mice treated with Vorapaxar and MRSA (Fig. 7I–J). In summary, pharmacological inhibition of PAR1 in mice significantly reduces itch behaviors that drives skin damage during bacterial exposure.

DISCUSSION

The underlying mechanisms of itch during microbial exposure were not previously understood. Here, we established that human pathogen *S. aureus* induces robust itch and scratch-induced damage during epicutaneous exposure. By screening through bacterial genetic mutants *in vivo* (Table S1), we find V8 protease as necessary and sufficient for itch and alloknesis. *S. aureus* V8 induced mouse and human pruriceptor neuron activation, which was mediated by host receptor PAR1. PAR1 inhibition prevented neuronal activation, itching, and skin damage. Our findings reveal a role for bacteria in causing itch and highlight the importance of the itch-scratch cycle in skin injury.

Given that *S. aureus* produces 10 proteases, it was striking that V8 protease specifically mediated itch. Staphopains A and B, Aureolysin, and SPLs did not contribute to itch. V8 is a serine protease with specificity to cleaving after glutamic acids, and in some conditions after aspartates[75]. V8 protease has been shown to be a dominant *S. aureus* virulence factor causing damage to keratinocytes[76]. Topical application of V8 increased TEWL and serum IgE levels in hairless mice[77]. A recent study profiled skin from healthy adults and AD patients for *S. aureus* virulence factors, and *sspA* transcript was detected in samples from both healthy and AD skin[78]. We found *sspA* transcript increased in AD compared to healthy skin. Reports have demonstrated that nearly all *S. aureus* isolates contain the *sspA* gene[79–81]. Antibodies specific to V8 can be detected from humans who have previously been infected with *S. aureus* and in the general population[82,83].

In addition to V8, *S. aureus* Hla activated DRG neurons and induced itch and pain when injected. PSMs can also cause itch and pain when injected into the mouse cheek[84]. While Hla and PSMs can induce itch, we found no difference in spontaneous itch or alloknesis in mice inoculated with *S. aureus* deficient in these toxins (Fig. 2). Levels of Hla and PSMs

produced by *S. aureus* on the skin surface maybe insufficient to induce itch. Matching this point, while *sspA* transcripts were high at day-5 following MRSA inoculation, we did not observe increased *psma1* or *hla* transcripts (Fig. 3). How *S. aureus* regulates expression of these factors on skin surface remains to be determined.

Non-microbial proteases have been linked to itch. Our study adds a bacterial protease as a pruritogen that acts through PAR1. Many previous reports have focused on the action of proteases on PAR2 and PAR4 in itch[45]. Plant proteases including cowhage mucanain, bromelain, and papain induce itch by acting via PAR2 and PAR4. Keratinocytes and immune cells express cathepsin S, which can induce itch through PAR2 and PAR4. Mast cell tryptase and chymase can also induce itch. A recent report found that mast cell tryptase activates PAR1 to cause anaphylaxis[85]. Keratinocytes produce kallikrein (KLK) proteases including KLK5 and KLK14 which can cleave PAR2[86] and drive itch[87,88] *S. aureus* can also induce keratinocyte expression of KLKs[89]. Our finding that PAR1 mediates itch during *S. aureus* exposure introduces this receptor as a driver of itch. PAR1 was expressed across several sensory neurons, including those expressing *Nppb, Mrpgra3*, and *S1pr3*[2,61]. In humans, its expression was more linked to $NPPB^+$ neurons[65]. How protease activation of $PAR1^+$ neuronal subsets induces signaling at the cellular level remains to be fully determined.

We observed that dermatitis at the site of bacterial exposure can be decoupled from itch and scratching behavior. PSMs and MYD88 were previously shown to drive inflammation following MRSA exposure[20,23]. We found that bacteria lacking PSMs caused decreased dermatitis but still induced itch; similarly, $Myd88^{-/-}$ mice showed decreased dermatitis, but still scratched. Therefore, itch and scratching behavior do not require pre-existing inflammation and skin barrier disruption. Our results indicate that V8 acts directly through neuronal PAR1 to induce itch independent of inflammation.

The role of other microbial proteases in itch requires further investigation. Bacteria produce numerous proteases that have various roles in health and disease[90]. *Staphylococcus epidermidis*, an opportunistic pathogen frequently found on healthy and AD skin, makes the protease EcpA which causes skin damage in AD patients[91]. *Streptococcus pyogenes*, another skin pathogen, produces proteases including SpeB which impact skin infection[92]. Beyond bacteria, how fungi, viruses and parasites contribute to itch are unknown.

Neuronal sensing of pathogens can mediate early defense responses to infection through neurogenic inflammation[93]. Nociceptors release neuropeptides including calcitonin gene-related peptide (CGRP) or substance P (SP) to mediate vascular[94,95] and immune changes[96]. PAR1 activation on primary afferents can induce release of CGRP and SP, provoking neurogenic inflammation[97]. Neuronal PAR1 activation could therefore mediate quick and sustained depletion of neuropeptides from primary afferents and downstream immune modulation.

Pathogens may hijack itch and other neural reflexes for their advantage. *Mycobacterium tuberculosis* (Mtb) directly activate vagal nociceptor neurons through a sulfolipid SL-1 to mediate coughing in guinea pigs, which could facilitate pathogen transmission[98]. *S. aureus* induces itch and scratching behaviors which mediate skin damage. This may impact

bacterial spread deeper in the skin or result in dissemination to distant body sites. Scratching could also facilitate bacterial spread to other hosts. Further investigation into how bacteria induce maladaptive behaviors to mediate invasion and dissemination are needed.

We found that blocking PAR1 reduced itch in mice, and V8 activates and cleave human PAR1. Therefore, PAR1 could be an attractive candidate to target for itch therapies. Vorapaxar is currently FDA-approved for prevention of thrombotic cardiovascular events[72]. Future development of topical application of such PAR1 antagonists could avoid adverse events caused by systemic delivery. There is interest in intrathecal injection as a method to deliver therapeutic siRNAs to modulate gene expression in neurons[99]. Itch is a major cause of suffering for the many patients with pruritic diseases accompanied by microbial dysbiosis[15,19,100,101]. Targeting PAR1 or bacterial proteases including V8 may be promising approaches. Therefore, our study reveals a distinct bacterial-driven itch mechanism that contributes to skin pathology and may be targeted for therapeutic treatment of itch.

Limitations of Study

While our study shows that V8 protease mediates *S. aureus* induced itch and acts through PAR1 on pruriceptors, we cannot fully rule out indirect mechanisms by which V8 could act. V8 could activate endogenous mammalian proteases, which may in turn act on PAR1. V8 protease cleaves human pro-thrombin, although the activity of this cleavage product is unknown[102], and Thrombin is a PAR1 agonist that can be produced by keratinocytes[103]. Another limitation is that while PAR1 knockdown and pharmacological blockade by Vorapaxar greatly reduces itch caused by both V8 and *S. aureus* exposure, it does not completely abrogate itch down to baseline levels in animals injected with V8 protease (Fig 6–7). Therefore, V8 could partially induce itch via mechanisms independent of PAR1. We observed a reduction in skin bacterial load in mice inoculated with Δ*sspA* MRSA, suggesting a fitness defect. More studies are needed to understand how V8 promotes MRSA virulence. V8 protease may act directly on keratinocytes, immune cells, or other skin cells to drive inflammation and barrier damage. V8 might also synergize with other *S. aureus* factors such as PSMs to drive tissue damage, resulting in deeper infection and pain. Because pain behavior analysis is not optimized for mouse back, it is not currently possible to assess how pain contributes to this model. While the model of epicutaneous *S. aureus* inoculation is widely used for topical exposure, it involves occlusion by Tegaderm tape, and is self-limiting, which may not reflect *S. aureus* dynamics in human AD lesions. It also mimics aspects of infection such as bacterial epidermal invasion. Additional studies are needed to examine V8 protease and PAR1 in itch in the context of human *S. aureus* colonization and AD. It would be of interest to test if human DRG neurons responding to V8 protease can response to other pruritogens. Due to limitations in availability of human donors, we mainly utilized mouse DRG neurons in this study. Future studies with human neurons are needed to show what subsets of neurons can respond to V8 protease and mediation through PAR1.

STAR METHODS

RESOURCE AVAILABILITY

Lead contact—Please direct requests for further information, resources, and reagents to the lead contact, Isaac Chiu (Isaac_chiu@hms.harvard.edu).

Materials availability—Bacterial strains generated in this study are available upon signing a materials transfer agreement (MTA).

Data and code availability

- Microscopy data, flow cytometry data, and mouse behavior recordings will be shared by the lead contact upon request. This paper analyzes existing, publicly available single cell RNA-seq data. These accession numbers for the datasets are listed in the key resources table.
- This study did not generate any sequencing data or original code.
- Any additional information required to reanalyze the data reported in this paper is available from the lead contact upon request.

EXPERIMENTAL MODEL AND STUDY PARTICIPANT DETAILS

Mice—All animal experiments were approved by the Institutional Animal Care and Use Committee (IACUC) at Harvard Medical School under protocol numbers IS000000543 and IS000000546 and were conducted in accordance with National Institutes of Health (NIH) animal research guidelines. Mice were bred and housed in individually ventilated micro-isolator cages within a full barrier, specific pathogen-free animal facility at Harvard Medical School under a 12h light/dark cycle with *ad libitum* access to food and water. Age-matched littermate male and female mice were used for experiments.

C57/BL6 mice that were free of rodent pathogens and *Staphylococcus aureus* were purchased from Taconic Biosciences. C57/BL6J mice, Ai14 strain B6.Rosa26-stop(flox)-tdTomato (#007914) [104], *Myd88* knockout strain B6.129P2(SJL)-*Myd88*$^{tm1.1Defr}$/J (#009088) [105], *F2rl1* knockout strain B6.Cg-*F2rl1*^{tm1Mslb}/J (#004993) [106], mast cell deficient B6.Cg-*Kit*$^{W\text{-}Sh}$ mice (#030764), and *Trpv1*-Cre$^{+/+}$ B6.129-Trpv1$^{tm1(cre)Bbm}$/J strain (#017769) were obtained from the Jackson Laboratory (Bar Harbor, ME). *Rag2*$^{-/-}$ *Il2rg*$^{-/-}$ strain C57BL/6NTac.Cg-Rag2^{tm1Fwa} Il2rg^{tm1Wjl} was obtained from Taconic Biosciences. *F2r*-flox mice were generated previously[107]. *Trpv1*-Cre$^{+/+}$ mice were crossed with *F2r*-flox mice to generate *Trpv1*$^{\Delta F2r}$ mice. Balbc/J (#00651) and *Il4ra*$^{-/-}$ (#003514) strain BALB/c-Il4ra^{tm1Sz}/J were purchased from Jackson Laboratory (Bar Harbor, ME). *Mrgpr* knockout mice [108] were provided by Xinzhong Dong (Johns Hopkins University). *Nav1.8*-Cre mice [109] were provided by John Wood (University College London). *Nav1.8*-Cre$^{+/+}$ mice were crossed with Ai14 mice to generate Nav1.8^{tdTomato} mice. *F2r* knockout strain *B6.129S4-F2r*^{tm1Ajc}/J mice were obtained by recovery from cryopreservation from Jackson Laboratories (#002862).

Human subjects for skin swab collection—Experiments involving human subjects were done according to protocols approved by University of California, San Diego IRB (Project#140144). Written informed consent was obtained from all subjects. Swabs of surface microbiota from a 5 cm^2 area of the antecubital fossa skin of both left and right arms were collected from 14 healthy subjects and 13 patients with AD as previously described [91]. Demographic details including age, sex, and race are given in Table S3. For subjects with AD, swabs were collected from both lesional and non-lesional skin. Swabs were stored in tryptic soy broth (TSB) and 16.67% glycerol at −80°C with swab intact until follow-on analysis was performed.

Human DRG samples from organ donors—Human lumbar DRGs were obtained from organ donors in collaboration with Southwest Transplant Alliance, as previously described[65]. Demographic details including age, sex, and race are given in Table S3. Human DRGs were immediately frozen in pulverized dry-ice on-site for RNAScope analysis or immersed in N-methyl-D-glutamate-artificial cerebrospinal fluid (NMDG-aCSF) for subsequent calcium imaging experiments[110]. All tissue procurement procedures were approved by the institutional review board at University of Texas at Dallas.

METHOD DETAILS

Bacterial strains and culture—All procedures related to bacterial strains and infectious disease work were approved by the Committee on Microbiological Safety (COMS) at Harvard medical school and were conducted under Biosafety Level 2 protocols and guidelines. All *Staphylococcus aureus* strains used in this study are listed in the Key Resources Table. Bacteria were grown in tryptic soy broth (TSB) at 37°C and growth was monitored by measuring the optical density at 600 nm (OD_{600}). *S. aureus* CA-MRSA strains LAC/USA300 (wildtype, WT) and GFP-MRSA are previously described[12]. Δ*agr* and Δ*hla* MRSA were obtained from Dr. Victor Torres[111]. The Δ*psmα* Δ*psmβ* Δ*hld* (ΔPsms) MRSA strain was a gift from Dr. Michael Otto[112].

Deletions of aureolysin (Δ*aur*), staphopain A and staphopain B (Δ*scpA* Δ*sspB*) and SplA-F (Δ*spl::erm*) strains were generated as previously described[113]. The V8 protease deletion (Δ*sspA*) was generated using homologous recombination as previously described, resulting in an encoded small peptide MKGPR* in its place[114]. Complementation of Δ*sspA* was achieved by cloning *sspA* with 245 bp of the promoter sequence into a pLL29-derived vector where the tetracycline antibiotic resistance cassette was replaced with an erythromycin resistance cassette (pLL29erm)[115,116]. The resulting plasmid was integrated at the φ11 *attP* site in RN4220 using helper plasmid pLL2787 and moved into the Δ*sspA* strain by phage transduction. The resulting strains were PCR and sequence verified.

V8 protease activity assays—Activity assays for V8 protease were performed as previously described with some modifications[117]. Filtered supernatants were further concentrated with an Amicon Ultra-15 Centrifugal Filter (10 kDa cutoff), dialyzed in 20 mM Tris pH 7.4, and normalized to a protein concentration of 0.45 mg/mL by the Pierce BCA Protein Assay (ThermoFisher) before beginning the FRET assay.

Epicutaneous MRSA exposure and measurement of itch and inflammation— The murine model of epicutaneous *Staphylococcus aureus* exposure was adapted from[20,23]. Prior to MRSA application, mice were shaved and treated with chemical depilation to remove back fur. Two days after fur removal, a 1 cm^2 gauze piece of soaked with 100uL of bacterial suspension was placed onto the skin just below the shoulder blades and the animals were covered with Tegaderm occlusive tape. Control animals were treated with gauze soaked with 100uL sterile PBS. Mice were monitored daily and the Tegaderm tape and gauze were removed at the endpoint so that inflammation and itch could be measured.

***S, aureus* exposure site dermatitis:** Inflammation caused directly by bacterial exposure was measured immediately after tape and gauze removal (before mice were able to scratch the back skin). Four parameters (edema, skin scale, erythema, and thickness) were assigned a score from 0 (none) to 3 (severe) and these measurements were summed for a total score of between 0 to 12 per mouse (Fig. S1B).

Transepidermal water loss: Following skin score assessment, a Tewameter TM300 device (Courage and Khazaka Electronic GmbH) was used to record TEWL at the site of gauze placement on the skin.

Alloknesis: Mice were stimulated 9 times with a 0.07g von Frey filament on the back skin near the exposure site. Bouts of scratching that occurred immediately after stimulation were recorded as a response.

Spontaneous itch: Prior to MRSA exposure, mice were habituated to the infrared behavior observation box (iBOB). Following tape and gauze removal at the endpoint of exposure, mice were returned to their home cage for several hours and allowed to groom the skin/fur that was previously covered by tape. After grooming behaviors returned to baseline, mice were place in iBOB for 90 minutes of video recording. Bouts of scratching were counted by observers blinded to the treatment groups.

Scratch-induced skin damage: Immediately after tape and gauze removal, mice were photographed from above, returned to their home cage, and allowed to freely scratch the back skin for 7 hours. After scratching, mice were anesthetized and photographed. Blinded observers analyzed the images to measure the total shaved skin area and the skin area that appeared inflamed (including the infected lesion site and the surrounding scratched areas) using ImageJ. The area of damaged skin was calculated as the percentage of inflamed skin area out of the total shaved area.

Bacterial load: Mice were euthanized according to approved veterinary protocols and the back skin was dissected and placed in 1 mL sterile PBS and bead beaten for 10 min to homogenize the tissue. The resulting tissue homogenate was serially diluted and plated on CHROMagar (Hardy Diagnostics) supplemented with 5.2 μg/mL cefoxitin to enumerate MRSA CFU.

Histology—Mice were euthanized by CO_2 inhalation and the back skin was dissected and fixed for 24h at 4°C in 4% paraformaldehyde. Fixed skin samples were embedded

with paraffin, sectioned, and stained with hematoxylin and eosin (H&E) dyes by the Harvard Medical School Rodent Histopathology Core. Stained sections were imaged by light microscopy on an Eclipse Ti-S/L100 inverted microscope (Nikon) and images collected by NIS-Elements AR software.

Subcutaneous MRSA infection—Mice were injected subcutaneously with 50μL of 10^7 CFU of MRSA in PBS. At 5-days post-infection, mice developed large dermonecrotic lesions at the infection site. Alloknesis was assessed by stimulating the skin close to the necrotic tissue. Spontaneous itch was measured by counting bouts of scratching to both the infected area and the healthy back skin surrounding the lesion.

Whole mount confocal microscopy—*Nav1.8*^{tdTomato} mice were treated epicutaneously with GFP-MRSA or sterile PBS. At 5 days post-treatment, mice were euthanized following approved veterinary protocols and the skin was dissected and fixed for 24h at 4°C in 4% paraformaldehyde. Following fixation, the skin was imaged using a Leica Stellaris 8 confocal microscope.

Mouse skin RNA isolation and quantitative real-time PCR—Mouse skin tissue was placed into TRIzol reagent (thermos Fisher) and homogenized by bead beating for 10 min. RNA was isolated using the Direct-zol RNA MiniPrep Plus kit according to manufacturer's instructions (Zymo Research). RNA was reverse-transcribed using the iScript cDNA synthesis kit (Bio-Rad). Primers (*sspA* primers sspA-F AND sspA-R, *psmA1* primers psmA1-F and psmA1-R, and *hla* primers hla-F and hla-R) and cDNA were mixed with Power SYBR green PCR master mix (Life Technologies) and qPCR was performed using a QuantStudio Real-Time PCR instrument (Thermo Fisher).

Human skin swab RNA isolation quantitative real-time PCR—RNA was isolated using the Purelink RNA isolation kit according to manufacturer's instructions (Thermo Fisher Scientific). For human swabs, 250μL of sample was removed from collection tubes and added to 500μL of RNA Protect Bacteria Reagent (Qiagen) for 10min at RT, then pelleted (13,000RPM, 10', RT). Pellet was resuspended with 700μL of RNA lysis buffer with 1% Beta-mercaptoethanol followed by column-based isolation of RNA. RNA was reverse-transcribed using the iScript cDNA synthesis kit (Bio-Rad). qPCR reactions were run on a CFX96 Real-Time Detection System (Bio-Rad) with cDNA, 2x SYBR Green qPCR Master Mix, and *sspA* specific primers sspA-F and sspA-R previously described[78].

Cheek injections and measurement of itch and pain—Mouse cheeks were shaved 2 days before experiments and were habituated for 30 minutes in iBOB chambers. Male and female mice were injected intradermally in the cheek with 20μL of PBS, V8 protease (40U), histamine (100μg), or capsaicin (40μg). For injections with antagonists, V8 protease was mixed with vorapaxar, SCH79797, or BMS986120 30 minutes prior to injection. Immediately after injection, mice were place into iBOB chambers and recovered for 30 minutes. Itch and pain behaviors were scored by blinded observers.

Alloknesis—The napes of mouse necks were shaved 2 days before experiments and mice were habituated in alloknesis chambers for 1 hour. Mice were injected intradermally in

the upper back with 50μL of PBS, V8 protease (40U), or histamine (100μg). The skin surrounding the injection site was mechanically stimulated for 1 second 3 times in a row with a 0.07g Von Frey filament, and this was repeated 3 times for a total of 9 stimulations.

KERTr cell culture and adherence assays—KERTr immortalized human keratinocytes were obtained from the American Type Culture Collection (#CRL-2309) and maintained in keratinocyte serum-free medium (Gibco #17005-042) with added Keratinocytes Supplements (Gibco #37000-015) including bovine pituitary extract (BPE; Gibco 13028-014) and human recombinant epidermal growth factor (EGF, Gibco #10450-013) and further supplemented with 35 ng/mL human recombinant epidermal growth factor (EGF; BD #354052).

Assays to quantify cell surface-adherent bacteria were performed as previously described[118]. Briefly, MRSA strains were grown to mid-log phase to infect confluent cell monolayers (multiplicity of infection [MOI], 1). Following a 30 min incubation, cells were treated with trypsin and lysed with 0.025% Triton X-100. The lysates were then serially diluted and plated on tryptic soy agar (TSA) to enumerate bacterial CFU. Experiments were performed four times with four replicates per MRSA strain, and results from a representative experiment are shown in Fig. S5D.

Expression and purification of recombinant PAR1 N-terminus—A codon-optimized sequence of human PAR1A22-T102 with a starting methionine was cloned into vector pTEV20 at the BspQ1 site[119]. The construct was transformed into *E. coli* BL21-Rosetta cells (Novagen) and grown overnight in LB supplemented with ampicillin (100 μg/mL) and chloramphenicol (10 μg/mL) at 37 °C. Overnight was subcultured at a 1:8 dilution in Terrific Broth (TB, BD Difco) supplemented with ampicillin (100 μg/mL) and chloramphenicol (10 μg/mL) and grown at 37 °C shaking at 220 RPM to a cell density of OD600 0.8-1.0 as measured in a cuvette with 1 cm pathlength. Isopropyl β-D-1-thiogalactopyranoside (IPTG) was added at a final concentration of 1 mM, and the culture was incubated at 25 °C for 2 hours. Cells were then centrifuged at 3,900 *x g* in an Eppendorf 5810R centrifuge set at 4 °C for 30 minutes. Centrifuged cell paste was stored at −80 °C. For purification, thawed cell paste was resuspended in Buffer A (0.1 M sodium phosphate buffer, pH 7.8, 0.2 M NaCl, 6 M urea) at a ratio of 5 mL buffer: 1 g cell mass, and cells were lysed by pushing lysate through a 28G needle attached to a syringe three times or until cells were lysed. Lysate was centrifuged at 3,900 *x g* in an Eppendorf 5810R centrifuge set at 4 °C for 30 minutes, and supernatant was filtered with a 0.45 μm filter. Filtered lysate was loaded onto a 5 mL HisTrap-FF column (Cytiva) equilibrated with Buffer A. A gradient of Buffer B (0.1 M sodium phosphate buffer, pH 7.8, 0.2 M NaCl, 0.5 M imidazole, 6 M urea) was applied from 0-100% over 10 column volumes (CV). $PAR1^{A22\text{-}T102}$-His_6 eluted at 41-56% Buffer B. Fractions were collected, dialyzed thrice in 1 L storage buffer (0.01 M sodium phosphate buffer pH 7.8, 6 M urea), and flash frozen in liquid nitrogen for storage at −80 °C.

Limited proteolysis of PAR1 N-terminus—Unless otherwise specified, tubes were incubated at room temperature for 10 min on a tube revolver (Thermo Scientific) set to 15 speed, and beads were separated from supernatant with a magnetic separation rack for 2

min (New England Biolabs). Per tube, 400 μL of Pierce™ Ni-NTA Magnetic Agarose Beads were equilibrated with storage buffer, and 1.5 mg of thawed PAR1 recombinant N-terminus was applied to the beads. Beads were washed thrice with storage buffer and thrice with reaction buffer (0.01 M sodium phosphate buffer, pH 7.8) to wash off unbound protein and renature N-terminus. V8 protease (E.C. 3.4.21.19, Sigma) was added at a concentration of 10 μg/mL V8 protease in 500 μL total volume, and reaction was incubated rotating for 30 minutes. Supernatant was removed and added to formic acid for a final concentration of 0.5% formic acid and immediately flash frozen. Resin beads were washed thrice with reaction buffer and incubated for 10 minutes with 400 μL elution buffer (0.01 M sodium phosphate buffer, pH 7.8, 500 mM imidazole). Supernatant was removed and added to formic acid for a final concentration of 2% formic acid and immediately flash frozen. Samples were submitted to Dr. Greg Sabat at the University of Wisconsin-Madison Mass Spectrometry Core for solid phase purification and LC-MS/MS analysis.

Mass Spectrometry—Samples were desalted using Pierce C-18 Tips, 100μl bed (ThermoFisher Scientific) per manufacturer protocol and eluted in 10μl of 70/30/0.1% ACN/H2O/TFA. Dried to completion in the speed-vac and finally reconstituted in 20μl of 0.1% formic acid / 3% ACN. Peptides were analyzed by nanoLC-MS/MS using the Agilent 1100 nanoflow system (Agilent) connected to hybrid linear ion trap-orbitrap mass spectrometer (LTQ-Orbitrap Elite™, Thermo Fisher Scientific) equipped with an EASY-Spray™ electrospray source (held at constant 35°C). Chromatography of peptides prior to mass spectral analysis was accomplished using capillary emitter column (PepMap® C18, 3μM, 100Å, 150x0.075mm, Thermo Fisher Scientific) onto which 2 μl of extracted peptides was automatically loaded. NanoHPLC system delivered solvents A: 0.1% (v/v) formic acid , and B: 99.9% (v/v) acetonitrile, 0.1% (v/v) formic acid at 0.50 μL/min to load the peptides (over a 30 minute period) and 0.3μl/min to elute peptides directly into the nano-electrospray with gradual gradient from 0% (v/v) B to 30% (v/v) B over 80 minutes and concluded with 5 minute fast gradient from 30% (v/v) B to 50% (v/v) B at which time a 5 minute flash-out from 50-95% (v/v) B took place. As peptides eluted from the HPLC-column/electrospray source survey MS scans were acquired in the Orbitrap with a resolution of 120,000 followed by CID-type MS/MS fragmentation of 30 most intense peptides detected in the MS1 scan from 350 to 1800 m/z; redundancy was limited by dynamic exclusion. Elite acquired MS/MS data files were converted to mgf file format using MSConvert (ProteoWizard: Open Source Software for Rapid Proteomics Tools Development). Resulting mgf files were used to search against Uniprot Escherichia coli reference database (UP000000625, 4,520 total sequences) appended with PAR1 (1-102 aa) protein along with a cRAP common lab contaminant database (116 total entries) using in-house Mascot search engine 2.7.0 [Matrix Science], assuming the digestion enzyme GluC, with fixed Cysteine carbamidomethylation and variable Methionine oxidation plus Asparagine or Glutamine deamidation. Peptide mass tolerance was set at 10 ppm and fragment mass at 0.6 Da. Protein annotations, significance of identification and spectral based quantification was done with Scaffold software (version 4.11.0, Proteome Software Inc., Portland, OR). Peptide identifications were accepted if they could be established at greater than 60.0% probability to achieve an FDR less than 1.0% by the Scaffold Local FDR algorithm. Protein identifications were accepted if they could be established at greater than 98.0% probability to achieve an FDR less than 1.0% and

contained at least 2 identified peptides. Protein probabilities were assigned by the Protein Prophet algorithm (Nesvizhskii, Al et al Anal. Chem. 2003;75(17):4646-58). Proteins that contained similar peptides and could not be differentiated based on MS/MS analysis alone were grouped to satisfy the principles of parsimony. Proteins sharing significant peptide evidence were grouped into clusters.

Culturing and calcium imaging of mouse DRG neurons—One day prior to calcium imaging, DRGs from male and female mice were collected and digested using a mixture of 2.5mg/mL Collagenase A and 1mg/mL Dispase II for 40 min. A single cell suspension was obtained by triturating the samples through 18G, 21G, and 26G needles. Neurons were separated from other cells and debris using BSA gradient and plated onto laminin-coated 35mm dishes or 96-well plates in Neural Basal Medium (NBM) (Thermo Fisher) supplemented with B27 serum-free supplement (Invitrogen), L-Glutamine (Invitrogen), Pen/Strep (Cellgro), and 25ng/mL NGF (Invitrogen).

Neurons were cultured overnight at 37C with 5% CO_2, then loaded with 5μM Fura-2-AM in NBM for 30 min. For experiments with histamine, chloroquine, S1P, and capsaicin, neurons were washed with Krebs-Ringer buffer (KR) (Boston BioProducts) and 100μL of KR, V8 (69.2μM), histamine (100μM), chloroquine (1mM), S1P (1μM), capsaicin (1μM), and KCl (100μM) were sequentially pipetted into the 35mm dish. Images were acquired with alternating 340/380 nm excitation wavelengths using a Nikon Eclipse Ti inverted microscope and Zyla sCMOS camera (Andor). For experiments with Hla, fMLF, and V8 protease, neurons were washed with KR and 100μL of KR, V8, Hla, fMLF, and KCl were sequentially pipetted onto the cells. Ratiometric analysis of 340/380 signal intensities was performed as described in[14]. For V8 dose-response experiments, calcium imaging of neurons in 96-well plates was performed as described in [120].

Culturing and calcium imaging of human neurons—Human lumbar DRGs were cleaned of any fat and connective tissue surrounding the ganglion. The protocol for the dissociation of DRGs for calcium imaging was inspired by [121]. The DRG was cut into roughly 1-2 mm chunks and immersed in pre-warmed 5 ml enzyme solution containing 2 mg/ml STEMxyme I (Worthington, LS004106) and 0.1 mg/ml DNAse I (Worthington, LS002139) in HBSS without calcium and magnesium (ThermoFisher, 14170161). The tissue-enzyme solution was gently and constantly mixed at 37°C in a shaking water bath. The tissue was triturated every 20 min using fire-polished glass pipette until a roughly homogenous solution was obtained (about 40 min). This mixture was passed through a 100 μm cell strainer (Corning, 352360) and the flow-through was layered onto 3ml of 10% bovine serum albumin density gradient. The resulting solution was centrifuged for 900 x g for 5 min at room temperature. The supernatant was removed and the pellet was resuspended in BrainPhys media (STEMCell, 05790) containing 1% penicillin-streptomycin (ThermoFisher, 15070063), 1% N2-A (STEMCell, 07152), 2% SM1 (STEMCell, 05711) and 1% GlutaMax (ThermoFisher, 35050061). Cells were plated onto 35 mm dishes that were pre-coated with poly-D-lysine (>300,000, Sigma Aldrich, P7405) overnight and then coated with laminin from human placenta (Sigma Aldrich, L6274) for 2-3 hours at 37°C

right before culturing. Cells were initially cultured for 2 hours in a 50μl droplet followed by immersion in 2 ml of pre-warmed BrainPhys media.

Calcium imaging with Fluo-4 AM was performed 24 hours after plating. Fluo-4 AM (ThermoFisher, F14201) was reconstituted in 2% of Pluronic F-127 (20% in DMSO, ThermoFisher, P3000MP) in BrainPhys Imaging media (STEMCell, 05796). Cells were loaded with Fluo-4 AM (1:100) for 30 min prior to imaging. The Fluo-4 AM solution was replaced with 2mL of pre-warmed BrainPhys Imaging media. Cells were imaged at 20X on an Olympus IX73 inverted microscope and data was acquired using the MetaFluor software (Olympus). A 120 second baseline was acquired prior to the addition of V8 protease (2 mg/ml, Worthington, LS003605), capsaicin (400nM) at 500 seconds, and KCl (50mM) at 700 seconds for a total imaging time of 840 seconds. Cells with an increase in the intracellular Fluo-4 signal over 10% of their baseline were deemed to be responsive to V8 administration. Only cells that responded to KCl (50 mM) were used in the analysis. Calcium imaging was performed on cells from DRGs from two donors (see Table S3).

RNAscope of mouse DRGs—Mouse samples for RNAScope were prepared as previously described[122]. Briefly, mouse DRGs were embedded in OCT and sectioned at 16μm on a cryostat. Sections were stored in −80C for 24 hrs, then brough to room temperature and fixed with 4% paraformaldehyde. In situ hybridization with *F2r* and *Tubb3* probes was performed using the RNAscope Multiplex V2 kit (ASD) according to manufacturer's instructions. All tissues were also tested with negative and positive control probe cocktails (ACD). Sections were imaged on a Leica Stellaris 8 confocal microscope.

RNAscope of human DRGs—Human samples for RNAScope were prepared as previously described [65]. Frozen human DRG samples were gradually embedded in OCT in a cryomold. Tissue was cryosectioned at 20μm, thawing momentarily in order to adhere to the slide. In situ hybridization using the RNAscope Multiplex V2 kit (ACD) was performed according to the manufacturer's recommendations and with Akoya fluorescein, Cy3, Cy5 dyes, as previously described[65]. All tissues were tested against a positive control probe cocktail (ACD) containing mRNAs with high, medium, and low expressions. Negative control probe against the bacterial DapB gene (ACD) was also used.

DRG sections were imaged on Olympus FV3000 confocal microscope at 20X or 40X magnification as per previously published parameters[65]. Background lipofuscin was identified as large globular intracellular structures that autofluoresced at 488, 550, and 647 wavelengths. Lipofuscin was not analyzed. Three 20X images were obtained from each human DRG section, and three sections were imaged per human donor. Images were analyzed using Olympus CellSens software (v1.18) as previously described[65]. Pie charts represent the average percentage of neurons that express each target from all donors (see Table S3). Probes used in this study: HS-F2R-C2 (ACD, 471081-C2), HS-TRPV1-C3 (ACD, 415381-C3), Hs-NPPB-C1 (ACD, 448511).

Luciferase-based PAR cleavage assays—CHO-K1 cells stably transfected with nLuc-PAR1-eYFP, nLuc-PAR2-eYFP, and nLuc-PAR4-eYFP pcDNA3.1(+) plasmids separately were seeded in a 96-well cell culture plate (flat-clear bottom, polystyrene, Nunc,

ThermoFisher Scientific) at a density of 1×10^4 cells per well and cultured for 48 h in Ham's F-12 (1×) Nutrient Mix (Gibco ThermoFisher Scientific) supplemented with 1 mM L-Glutamine, 100 U/ml penicillin, 100 μg/mL streptomycin, 1 mM sodium pyruvate, 10% v/v heat inactivated Fetal Bovine Serum (FBS), and 600 μg/mL geneticin selective antibiotic (G418 Sulfate, Gibco® ThermoFisher Scientific). The cells were rinsed with HBSS (100 μL × 3) and incubated with 100 μL HBSS at 37°C for 15 minutes. Cell supernatant (50 μL) was aliquoted into a white 96-well plate (polystyrene, Nunc, ThermoFisher Scientific) to measure the basal luminescence. The cells were further incubated with 50 μL V8 protease or controls in a half-log scale concentrations at 37°C for 15 minutes, and 50 μL of cell supernatant from each well was aliquoted as before. Furimazine (2 μl/mL, Promega) was added and the nLuc cleavage of the receptor was measured on Mithras LB 940 (Berthold Technologies, measurement time: 1 s per well) plate reader. The luminescence measurements of the samples were normalized by subtracting the basal luminescence. The concentration-effect curves were plotted and analyzed using the dose-response stimulation three parameters model and the $\log^{10}$EC50 ± SEM values were obtained on GraphPad Prism 8.

PAR1 calcium signaling in HEK-293 cells—HEK-293 cells (0.01x10^6) were plated in poly-d-lysine coated black walled clear bottom 96 well plates (Nunc) and cultured for 48 h in DMEM containing 10% FBS (Gibco). Media was removed and cells were incubated with the calcium indicator Fluo-4 NW (Thermo Fisher Scientific) at 37°C for 30 minutes and for a further 15 minutes at room temperature in the dark. Agonists were added and Ca2+ mobilization induced change in fluorescence (λEx/Em 494/516 nm) was measured in real time using a FlexStation3 microplate reader (Molecular Devices). The total run time for each spectrum was 180 s with baseline recorded for 20 s prior to the addition of agonists. To measure disarming of PAR1, cells were incubated with V8 for 15 minutes before measuring thrombin and TFLLR-NH_2 stimulated responses. (A23187, 6 μM, Sigma-Aldrich) was used as a control to ensure equivalent levels of Fluo-4 NW loading in each well.

PAR1 cleavage at HEK cell membrane—Dually tagged PAR1 in HEK cells was used as previously described[123]. Cells were placed in growth media containing E64 (5uM) and heparin (5 units/ml). After 1h stimulation, cells were fixed with 10% buffered formalin, and images were recorded with confocal microscope (Infinity image facility, Toulouse, France).

Skin cell preparation and flow cytometry—Skin from mice injected intradermally with PBS or V8 protease were obtained 30 minutes after injection. Cells were isolated and stained for flow cytometry as previously described[44]. Cells were preincubated with the Fcγ receptor–specific blocking mAb (clone 2.4G2, BioLegend) and washed before staining mAbs and analysis on LSR Fortessa (BD Biosciences). Data were analyzed with FlowJo software.

Intrathecal siRNA injection—Intrathecal delivery of siRNA was performed as in [37]. Briefly, siRNA purchased from Thermo Scientific were mixed with In Vivo JetPEI (Polyplus Transfection) according to the manufacturer's protocol. The N:P ratio used was 6. Mice

were injected intrathecally between L5 and L6 spinal levels with 5μL volume for 3 days in a row prior to itch experiments.

Mouse DRG RT-qPCR—One day after the last intrathecal siRNA injection, thoracic DRGs were dissected out of mice and placed in RNAprotect reagent (Qiagen). Tissues were homogenized by beadbeating with 0.1mm silica beads, RNA was extracted with the NucleoSpin RNA isolation kit (Macherey Nagel) and converted to cDNA with the iScript cDNA synthesis kit (Bio-Rad) following manufacturer's instructions. Primers (*il31ra* primers il31ra-F and il31ra-R, or *f2r* primers f2r-F, f2r-R) and cDNA were mixed with Power SYBR green PCR master mix (Life Technologies) and qPCR was performed using a QuantStudio Real-Time PCR instrument (Thermo Fisher).

Oral Vorapaxar treatment—Mice were gavaged daily with 100μL volume of either vehicle or Vorapaxar solution starting 2-days prior to *S. aureus* topical application and until the endpoint of 5 days.

QUANTIFICATION AND STATISTICAL ANALYSIS

Analysis of data was performed using GraphPad Prism version 9.5.1 (GraphPad Software). Comparison of data between two groups was performed using Mann-Whitney tests. Comparison of data between more than two groups with one independent variable was performed using one-way ANOVA with Tukey's multiple comparisons tests. Comparison of two independent variables was performed using two-way ANOVA with Tukey's multiple comparisons tests. P-values of less than 0.05 were considered statistically significant. Statistical details including statistical tests used, number of samples (n), and P-values are reported in figure legends.

Supplementary Material

Refer to Web version on PubMed Central for supplementary material.

ADKNOWLEDGEMENTS

We thank Gabriel Nunez (U. Michigan) and Matsumoto Masanori for teaching us the epicutaneous MRSA model. We thank Michael Otto (NIH) for providing ΔPsms strain of MRSA. We thank Larissa Staurengo-Ferrari, Daping Yang, Himanish Basu, Felipe Pinho-Ribeiro, Antonia Wallrapp, Glendon Wu, Jon Sautter, Brian Kim, Dan Kaplan, and Heidi Kong for helpful discussions. We thank Lora Bankova for calcium imaging support. We thank Jorge C. Escalante-Semerena for the pTEV20 vector for expression of PAR1 recombinant N-terminus, Greg Sabat (U. Wisconsin-Madison Mass Spectrometry Core) for mass spectrometry and analysis. We thank Dana-Farber/Harvard Cancer Center (supported by NIH/NCI 5P30CA06516) Rodent Histopathology Core. We thank Inserm U1291 Image Core Facility. We are grateful to organ donors and their families for the gift of life and research provided by their organ donation. We thank Dr. Geoffrey Funk and Anna Cervantes at Southwest Transplant Alliance for surgical extraction of human DRGs. Graphical abstract and figure schematics were created with Biorender.com. This study was supported by funding from NIH R01AI168005 (NIAID) to A.R.H and I.M.C; Food Allergy Science Initiative to I.M.C.; Burroughs Wellcome Fund to I.M.C.; Drako Family Fund to I.M.C.; Jackson-Wijaya Research Fund to I.M.C.; R01AI153185 (NIAID) to A.R.H; Canadian Institutes of Health Research (CIHR) grant 376560 and 469411 to R.R.; NIH R01NS065926, R01NS102161, R01NS111929 (NINDS) to T.J.P.; NIH R37AI052453, R01AR076082, U01AI152038, UM1AI151958 to R.G.; NIH R01AI153185 to R.G. and A.R.H., NIH R01JL160582 to J.S.P.; NIH F32AI172080 to F.C.; NIH T32AI049928 to A.F.; ANR-PARCURE PRCE-CE18, 2020 to N.V.; and NIH 1R21AG075419 to B.J.W.

INCLUSION AND DIVERSITY

We worked to ensure gender balance in the recruitment of human subjects. We worked to ensure ethnic or other types of diversity in the recruitment of human subjects. We worked to ensure sex balance in the selection of non-human subjects.

REFERENCES

1. LaMotte RH, Dong X, and Ringkamp M (2014). Sensory neurons and circuits mediating itch. Nat Rev Neurosci 15, 19–31. 10.1038/nrn3641. [PubMed: 24356071]
2. Bautista DM, Wilson SR, and Hoon MA (2014). Why we scratch an itch: the molecules, cells and circuits of itch. Nat Neurosci 17, 175–182. 10.1038/nn.3619. [PubMed: 24473265]
3. Wang F, and Kim BS (2020). Itch: A Paradigm of Neuroimmune Crosstalk. Immunity 52, 753–766. 10.1016/j.immuni.2020.04.008. [PubMed: 32433948]
4. Hwang J, Jaros J, and Shi VY (2020). Staphylococcus aureus in Atopic Dermatitis: Past, Present, and Future. Dermatitis 31, 247–258. 10.1097/DER.0000000000000589. [PubMed: 32209864]
5. Campione E, Lanna C, Diluvio L, Cannizzaro MV, Grelli S, Galluzzo M, Talamonti M, Annicchiarico-Petruzzelli M, Mancini M, Melino G, et al. (2020). Skin immunity and its dysregulation in atopic dermatitis, hidradenitis suppurativa and vitiligo. Cell Cycle 19, 257–267. 10.1080/15384101.2019.1707455. [PubMed: 31905036]
6. Geoghegan JA, Irvine AD, and Foster TJ (2018). Staphylococcus aureus and Atopic Dermatitis: A Complex and Evolving Relationship. Trends Microbiol 26, 484–497. 10.1016/j.tim.2017.11.008. [PubMed: 29233606]
7. Kim K. (2012). Neuroimmunological mechanism of pruritus in atopic dermatitis focused on the role of serotonin. Biomol Ther (Seoul) 20, 506–512. 10.4062/biomolther.2012.20.6.506. [PubMed: 24009842]
8. Blicharz L, Usarek P, Mlynarczyk G, Skowronski K, Rudnicka L, and Samochocki Z (2020). Is Itch Intensity in Atopic Dermatitis Associated with Skin Colonization by Staphylococcus aureus? Indian J Dermatol 65, 17–21. 10.4103/ijd.IJD_136_19. [PubMed: 32029934]
9. Seilie ES, and Bubeck Wardenburg J (2017). Staphylococcus aureus pore-forming toxins: The interface of pathogen and host complexity. Semin Cell Dev Biol 72, 101–116. 10.1016/j.semcdb.2017.04.003. [PubMed: 28445785]
10. Pietrocola G, Nobile G, Rindi S, and Speziale P (2017). Staphylococcus aureus Manipulates Innate Immunity through Own and Host-Expressed Proteases. Front Cell Infect Microbiol 7, 166. 10.3389/fcimb.2017.00166. [PubMed: 28529927]
11. Hatlen TJ, and Miller LG (2021). Staphylococcal Skin and Soft Tissue Infections. Infect Dis Clin North Am 35, 81–105. 10.1016/j.idc.2020.10.003. [PubMed: 33303329]
12. Chiu IM, Heesters BA, Ghasemlou N, Von Hehn CA, Zhao F, Tran J, Wainger B, Strominger A, Muralidharan S, Horswill AR, et al. (2013). Bacteria activate sensory neurons that modulate pain and inflammation. Nature 501, 52–57. 10.1038/nature12479. [PubMed: 23965627]
13. Blake KJ, Baral P, Voisin T, Lubkin A, Pinho-Ribeiro FA, Adams KL, Roberson DP, Ma YC, Otto M, Woolf CJ, et al. (2018). Staphylococcus aureus produces pain through pore-forming toxins and neuronal TRPV1 that is silenced by QX-314. Nat Commun 9, 37. 10.1038/s41467-017-02448-6. [PubMed: 29295977]
14. Pinho-Ribeiro FA, Baddal B, Haarsma R, O'Seaghdha M, Yang NJ, Blake KJ, Portley M, Verri WA, Dale JB, Wessels MR, and Chiu IM (2018). Blocking Neuronal Signaling to Immune Cells Treats Streptococcal Invasive Infection. Cell 173, 1083–1097 e1022. 10.1016/j.cell.2018.04.006. [PubMed: 29754819]
15. Harrison IP, and Spada F (2019). Breaking the Itch-Scratch Cycle: Topical Options for the Management of Chronic Cutaneous Itch in Atopic Dermatitis. Medicines (Basel) 6. 10.3390/medicines6030076.
16. Kwatra SG (2020). Breaking the Itch-Scratch Cycle in Prurigo Nodularis. N Engl J Med 382, 757–758. 10.1056/NEJMe1916733. [PubMed: 32074425]

17. Elewski B, Alexis AF, Lebwohl M, Stein Gold L, Pariser D, Del Rosso J, and Yosipovitch G (2019). Itch: an under-recognized problem in psoriasis. J Eur Acad Dermatol Venereol 33, 1465–1476. 10.1111/jdv.15450. [PubMed: 30680819]

18. Ross SE (2011). Pain and itch: insights into the neural circuits of aversive somatosensation in health and disease. Curr Opin Neurobiol 21, 880–887. 10.1016/j.conb.2011.10.012. [PubMed: 22054924]

19. Yosipovitch G, Greaves MW, and Schmelz M (2003). Itch. Lancet 361, 690–694. 10.1016/S0140-6736(03)12570-6. [PubMed: 12606187]

20. Liu H, Archer NK, Dillen CA, Wang Y, Ashbaugh AG, Ortines RV, Kao T, Lee SK, Cai SS, Miller RJ, et al. (2017). Staphylococcus aureus Epicutaneous Exposure Drives Skin Inflammation via IL-36-Mediated T Cell Responses. Cell Host Microbe 22, 653–666 e655. 10.1016/j.chom.2017.10.006. [PubMed: 29120743]

21. Patrick GJ, Liu H, Alphonse MP, Dikeman DA, Youn C, Otterson JC, Wang Y, Ravipati A, Mazhar M, Denny G, et al. (2021). Epicutaneous Staphylococcus aureus induces IL-36 to enhance IgE production and ensuing allergic disease. J Clin Invest 131. 10.1172/JCI143334.

22. Nakatsuji T, Hata TR, Tong Y, Cheng JY, Shafiq F, Butcher AM, Salem SS, Brinton SL, Rudman Spergel AK, Johnson K, et al. (2021). Development of a human skin commensal microbe for bacteriotherapy of atopic dermatitis and use in a phase 1 randomized clinical trial. Nat Med 27, 700–709. 10.1038/s41591-021-01256-2. [PubMed: 33619370]

23. Nakagawa S, Matsumoto M, Katayama Y, Oguma R, Wakabayashi S, Nygaard T, Saijo S, Inohara N, Otto M, Matsue H, et al. (2017). Staphylococcus aureus Virulent PSMα Peptides Induce Keratinocyte Alarmin Release to Orchestrate IL-17-Dependent Skin Inflammation. Cell Host Microbe 22, 667–677.e665. 10.1016/j.chom.2017.10.008. [PubMed: 29120744]

24. Moran GJ, Krishnadasan A, Gorwitz RJ, Fosheim GE, McDougal LK, Carey RB, and Talan DA (2006). Methicillin-resistant S. aureus infections among patients in the emergency department. N Engl J Med 355, 666–674. 10.1056/NEJMoa055356. [PubMed: 16914702]

25. Andersen HH, Akiyama T, Nattkemper LA, van Laarhoven A, Elberling J, Yosipovitch G, and Arendt-Nielsen L (2018). Alloknesis and hyperknesis-mechanisms, assessment methodology, and clinical implications of itch sensitization. Pain 159, 1185–1197. 10.1097/j.pain.0000000000001220. [PubMed: 29659469]

26. Ikoma A, Fartasch M, Heyer G, Miyachi Y, Handwerker H, and Schmelz M (2004). Painful stimuli evoke itch in patients with chronic pruritus: central sensitization for itch. Neurology 62, 212–217. 10.1212/wnl.62.2.212. [PubMed: 14745056]

27. Feng J, Luo J, Yang P, Du J, Kim BS, and Hu H (2018). Piezo2 channel-Merkel cell signaling modulates the conversion of touch to itch. Science 360, 530–533. 10.1126/science.aar5703. [PubMed: 29724954]

28. Akiyama T, Carstens MI, Ikoma A, Cevikbas F, Steinhoff M, and Carstens E (2012). Mouse model of touch-evoked itch (alloknesis). J Invest Dermatol 132, 1886–1891. 10.1038/jid.2012.52. [PubMed: 22418875]

29. Takanami K, Uta D, Matsuda KI, Kawata M, Carstens E, Sakamoto T, and Sakamoto H (2021). Estrogens influence female itch sensitivity via the spinal gastrin-releasing peptide receptor neurons. Proc Natl Acad Sci U S A 118. 10.1073/pnas.2103536118.

30. Rimoin LP, Kwatra SG, and Yosipovitch G (2013). Female-specific pruritus from childhood to postmenopause: clinical features, hormonal factors, and treatment considerations. Dermatol Ther 26, 157–167. 10.1111/dth.12034. [PubMed: 23551372]

31. Adams SC, Garner JP, Felt SA, Geronimo JT, and Chu DK (2016). A “Pedi” Cures All: Toenail Trimming and the Treatment of Ulcerative Dermatitis in Mice. PLoS One 11, e0144871. 10.1371/journal.pone.0144871. [PubMed: 26735497]

32. Dong X, and Dong X (2018). Peripheral and Central Mechanisms of Itch. Neuron 98, 482–494. 10.1016/j.neuron.2018.03.023. [PubMed: 29723501]

33. Oetjen LK, Mack MR, Feng J, Whelan TM, Niu H, Guo CJ, Chen S, Trier AM, Xu AZ, Tripathi SV, et al. (2017). Sensory Neurons Co-opt Classical Immune Signaling Pathways to Mediate Chronic Itch. Cell 171, 217–228.e213. 10.1016/j.cell.2017.08.006. [PubMed: 28890086]

34. Siracusa MC, Kim BS, Spergel JM, and Artis D (2013). Basophils and allergic inflammation. J Allergy Clin Immunol 132, 789–801; quiz 788. 10.1016/j.jaci.2013.07.046. [PubMed: 24075190]
35. Obata K, Mukai K, Tsujimura Y, Ishiwata K, Kawano Y, Minegishi Y, Watanabe N, and Karasuyama H (2007). Basophils are essential initiators of a novel type of chronic allergic inflammation. Blood 110, 913–920. 10.1182/blood-2007-01-068718. [PubMed: 17409268]
36. Garcovich S, Maurelli M, Gisondi P, Peris K, Yosipovitch G, and Girolomoni G (2021). Pruritus as a Distinctive Feature of Type 2 Inflammation. Vaccines (Basel) 9. 10.3390/vaccines9030303.
37. Silva CR, Melo BMS, Silva JR, Lopes AH, Pereira JA, Cecilio NT, Berlink J, Souza GG, Lucas G, Vogl T, et al. (2020). S100A9 plays a pivotal role in a mouse model of herpetic neuralgia via TLR4/TNF pathway. Brain Behav Immun 88, 353–362. 10.1016/j.bbi.2020.03.033. [PubMed: 32243898]
38. Shinkai Y, Rathbun G, Lam KP, Oltz EM, Stewart V, Mendelsohn M, Charron J, Datta M, Young F, Stall AM, and et al. (1992). RAG-2-deficient mice lack mature lymphocytes owing to inability to initiate V(D)J rearrangement. Cell 68, 855–867. 10.1016/0092-8674(92)90029-c. [PubMed: 1547487]
39. Cao X, Shores EW, Hu-Li J, Anver MR, Kelsall BL, Russell SM, Drago J, Noguchi M, Grinberg A, Bloom ET, and et al. (1995). Defective lymphoid development in mice lacking expression of the common cytokine receptor gamma chain. Immunity 2, 223–238. 10.1016/1074-7613(95)90047-0. [PubMed: 7697543]
40. Garibyan L, Rheingold CG, and Lerner EA (2013). Understanding the pathophysiology of itch. Dermatol Ther 26, 84–91. 10.1111/dth.12025. [PubMed: 23551365]
41. Akopian AN, Sivilotti L, and Wood JN (1996). A tetrodotoxin-resistant voltage-gated sodium channel expressed by sensory neurons. Nature 379, 257–262. 10.1038/379257a0. [PubMed: 8538791]
42. Sangameswaran L, Delgado SG, Fish LM, Koch BD, Jakeman LB, Stewart GR, Sze P, Hunter JC, Eglen RM, and Herman RC (1996). Structure and function of a novel voltage-gated, tetrodotoxin-resistant sodium channel specific to sensory neurons. J Biol Chem 271, 5953–5956. 10.1074/jbc.271.11.5953. [PubMed: 8626372]
43. Jenul C, and Horswill AR (2019). Regulation of Staphylococcus aureus Virulence. Microbiol Spectr 7. 10.1128/microbiolspec.GPP3-0031-2018.
44. Mack MR, and Kim BS (2018). The Itch-Scratch Cycle: A Neuroimmune Perspective. Trends Immunol 39, 980–991. 10.1016/j.it.2018.10.001. [PubMed: 30471983]
45. Akiyama T, Lerner EA, and Carstens E (2015). Protease-activated receptors and itch. Handb Exp Pharmacol 226, 219–235. 10.1007/978-3-662-44605-8_13. [PubMed: 25861783]
46. Gimza BD, Jackson JK, Frey AM, Budny BG, Chaput D, Rizzo DN, and Shaw LN (2021). Unraveling the Impact of Secreted Proteases on Hypervirulence in Staphylococcus aureus. mBio 12. 10.1128/mBio.03288-20.
47. Wörmann ME, Reichmann NT, Malone CL, Horswill AR, and Gründling A (2011). Proteolytic cleavage inactivates the Staphylococcus aureus lipoteichoic acid synthase. J Bacteriol 193, 5279–5291. 10.1128/jb.00369-11. [PubMed: 21784926]
48. Williams MR, Costa SK, Zaramela LS, Khalil S, Todd DA, Winter HL, Sanford JA, O'Neill AM, Liggins MC, Nakatsuji T, et al. (2019). Quorum sensing between bacterial species on the skin protects against epidermal injury in atopic dermatitis. Sci Transl Med 11. 10.1126/scitranslmed.aat8329.
49. Rice K, Peralta R, Bast D, de Azavedo J, and McGavin MJ (2001). Description of staphylococcus serine protease (ssp) operon in Staphylococcus aureus and nonpolar inactivation of sspA-encoded serine protease. Infect Immun 69, 159–169. 10.1128/iai.69.1.159-169.2001. [PubMed: 11119502]
50. Shimada SG, and LaMotte RH (2008). Behavioral differentiation between itch and pain in mouse. Pain 139, 681–687. 10.1016/j.pain.2008.08.002. [PubMed: 18789837]
51. Yamanoi Y, Kittaka H, and Tominaga M (2019). Cheek Injection Model for Simultaneous Measurement of Pain and Itch-related Behaviors. J Vis Exp. 10.3791/58943.
52. Chandrabalan A, and Ramachandran R (2021). Molecular mechanisms regulating Proteinase-Activated Receptors (PARs). Febs j 288, 2697–2726. 10.1111/febs.15829. [PubMed: 33742547]

53. Coughlin SR (2000). Thrombin signalling and protease-activated receptors. Nature 407, 258–264. 10.1038/35025229. [PubMed: 11001069]
54. Coughlin SR (2005). Protease-activated receptors in hemostasis, thrombosis and vascular biology. J Thromb Haemost3, 1800–1814. 10.1111/j.1538-7836.2005.01377.x. [PubMed: 16102047]
55. Nakanishi-Matsui M, Zheng YW, Sulciner DJ, Weiss EJ, Ludeman MJ, and Coughlin SR (2000). PAR3 is a cofactor for PAR4 activation by thrombin. Nature 404, 609–613. 10.1038/35007085. [PubMed: 10766244]
56. Chandrabalan A, Firth A, Litchfield RB, Appleton CT, Getgood A, and Ramachandran R (2020). Identification of Proteinase Activated Receptor (PAR) cleaving enzymes in human osteoarthritis knee joint synovial fluids. bioRxiv, 2020.2010.2021.336693. 10.1101/2020.10.21.336693.
57. Markert Y, Köditz J, Ulbrich-Hofmann R, and Arnold U (2003). Proline versus charge concept for protein stabilization against proteolytic attack. Protein Engineering, Design and Selection 16, 1041–1046. 10.1093/protein/gzg136.
58. Martin L, Augé C, Boué J, Buresi MC, Chapman K, Asfaha S, Andrade-Gordon P, Steinhoff M, Cenac N, Dietrich G, and Vergnolle N (2009). Thrombin receptor: An endogenous inhibitor of inflammatory pain, activating opioid pathways. Pain 146, 121–129. 10.1016/j.pain.2009.07.016. [PubMed: 19674841]
59. Desormeaux C, Bautzova T, Garcia-Caraballo S, Rolland C, Barbaro MR, Brierley SM, Barbara G, Vergnolle N, and Cenac N (2018). Protease-activated receptor 1 is implicated in irritable bowel syndrome mediators-induced signaling to thoracic human sensory neurons. Pain 159, 1257–1267. 10.1097/j.pain.0000000000001208. [PubMed: 29554016]
60. Bahou WF, Nierman WC, Durkin AS, Potter CL, and Demetrick DJ (1993). Chromosomal assignment of the human thrombin receptor gene: localization to region q13 of chromosome 5. Blood 82, 1532–1537. [PubMed: 8395910]
61. Zeisel A, Hochgerner H, Lonnerberg P, Johnsson A, Memic F, van der Zwan J, Haring M, Braun E, Borm LE, La Manno G, et al. (2018). Molecular Architecture of the Mouse Nervous System. Cell 174, 999–1014 e1022. 10.1016/j.cell.2018.06.021. [PubMed: 30096314]
62. Hill RZ, Morita T, Brem RB, and Bautista DM (2018). S1PR3 Mediates Itch and Pain via Distinct TRP Channel-Dependent Pathways. J Neurosci 38, 7833–7843. 10.1523/jneurosci.1266-18.2018. [PubMed: 30082422]
63. Akiyama T, and Carstens E (2013). Neural processing of itch. Neuroscience 250, 697–714. 10.1016/j.neuroscience.2013.07.035. [PubMed: 23891755]
64. Goswami SC, Thierry-Mieg D, Thierry-Mieg J, Mishra S, Hoon MA, Mannes AJ, and Iadarola MJ (2014). Itch-associated peptides: RNA-Seq and bioinformatic analysis of natriuretic precursor peptide B and gastrin releasing peptide in dorsal root and trigeminal ganglia, and the spinal cord. Mol Pain 10, 44. 10.1186/1744-8069-10-44. [PubMed: 25123163]
65. Tavares-Ferreira D, Shiers S, Ray PR, Wangzhou A, Jeevakumar V, Sankaranarayanan I, Cervantes AM, Reese JC, Chamessian A, Copits BA, et al. (2022). Spatial transcriptomics of dorsal root ganglia identifies molecular signatures of human nociceptors. Sci Transl Med 14, eabj8186. 10.1126/scitranslmed.abj8186. [PubMed: 35171654]
66. Kunitz M. (1947). ISOLATION OF A CRYSTALLINE PROTEIN COMPOUND OF TRYPSIN AND OF SOYBEAN TRYPSIN-INHIBITOR. J Gen Physiol 30, 311–320. 10.1085/jgp.30.4.311. [PubMed: 19873497]
67. Frydrych I, and Mlejnek P (2008). Serine protease inhibitors N-alpha-tosyl-L-lysinyl-chloromethylketone (TLCK) and N-tosyl-L-phenylalaninyl-chloromethylketone (TPCK) are potent inhibitors of activated caspase proteases. J Cell Biochem 103, 1646–1656. 10.1002/jcb.21550. [PubMed: 17879947]
68. Chackalamannil S, Wang Y, Greenlee WJ, Hu Z, Xia Y, Ahn HS, Boykow G, Hsieh Y, Palamanda J, Agans-Fantuzzi J, et al. (2008). Discovery of a novel, orally active himbacine-based thrombin receptor antagonist (SCH 530348) with potent antiplatelet activity. J Med Chem 51, 3061–3064. 10.1021/jm800180e. [PubMed: 18447380]
69. Liu Q, and Dong X (2015). The role of the Mrgpr receptor family in itch. Handb Exp Pharmacol 226, 71–88. 10.1007/978-3-662-44605-8_5. [PubMed: 25861775]

70. Zhao J, Munanairi A, Liu XY, Zhang J, Hu L, Hu M, Bu D, Liu L, Xie Z, Kim BS, et al. (2020). PAR2 Mediates Itch via TRPV3 Signaling in Keratinocytes. J Invest Dermatol 140, 1524–1532. 10.1016/j.jid.2020.01.012. [PubMed: 32004565]
71. Warwick C, Cassidy C, Hachisuka J, Wright MC, Baumbauer KM, Adelman PC, Lee KH, Smith KM, Sheahan TD, Ross SE, and Koerber HR (2021). MrgprdCre lineage neurons mediate optogenetic allodynia through an emergent polysynaptic circuit. Pain 162, 2120–2131. 10.1097/j.pain.0000000000002227. [PubMed: 34130311]
72. Tantry US, Bliden KP, Chaudhary R, Novakovic M, Rout A, and Gurbel PA (2020). Vorapaxar in the treatment of cardiovascular diseases. Future Cardiol 16, 373–384. 10.2217/fca-2019-0090. [PubMed: 32308016]
73. Gupta N, Liu R, Shin S, Sinha R, Pogliano J, Pogliano K, Griffin JH, Nizet V, and Corriden R (2018). SCH79797 improves outcomes in experimental bacterial pneumonia by boosting neutrophil killing and direct antibiotic activity. J Antimicrob Chemother 73, 1586–1594. 10.1093/jac/dky033. [PubMed: 29514266]
74. Martin JK 2nd, Sheehan JP, Bratton BP, Moore GM, Mateus A, Li SH, Kim H, Rabinowitz JD, Typas A, Savitski MM, et al. (2020). A Dual-Mechanism Antibiotic Kills Gram-Negative Bacteria and Avoids Drug Resistance. Cell 181, 1518–1532.e1514. 10.1016/j.cell.2020.05.005. [PubMed: 32497502]
75. Prasad L, Leduc Y, Hayakawa K, and Delbaere LT (2004). The structure of a universally employed enzyme: V8 protease from Staphylococcus aureus. Acta Crystallogr D Biol Crystallogr 60, 256–259. 10.1107/s090744490302599x. [PubMed: 14747701]
76. Wang B, McHugh BJ, Qureshi A, Campopiano DJ, Clarke DJ, Fitzgerald JR, Dorin JR, Weller R, and Davidson DJ (2017). IL-1β-Induced Protection of Keratinocytes against Staphylococcus aureus-Secreted Proteases Is Mediated by Human β-Defensin 2. J Invest Dermatol 137, 95–105. 10.1016/j.jid.2016.08.025. [PubMed: 27702565]
77. Iida H, Takai T, Hirasawa Y, Kamijo S, Shimura S, Ochi H, Nishioka I, Maruyama N, Ogawa H, Okumura K, and Ikeda S (2014). Epicutaneous administration of papain induces IgE and IgG responses in a cysteine protease activity-dependent manner. Allergol Int 63, 219–226. 10.2332/allergolint.13-OA-0621. [PubMed: 24662805]
78. Poh SE, Koh WLC, Lim SYD, Wang ECE, Yew YW, Common JEA, Oon HH, and Li H (2022). Expression of Staphylococcus aureus Virulence Factors in Atopic Dermatitis. JID Innov 2, 100130. 10.1016/j.xjidi.2022.100130. [PubMed: 35860448]
79. Kot B, Piechota M, Jakubczak A, Gryzińska M, Witeska M, Grużewska A, Baran K, and Denkiewicz P (2022). The prevalence of virulence determinants in methicillin-resistant Staphylococcus aureus isolated from different infections in hospitalized patients in Poland. Sci Rep 12, 5477. 10.1038/s41598-022-09517-x. [PubMed: 35361858]
80. Khan S, Marasa BS, Sung K, and Nawaz M (2021). Genotypic Characterization of Clinical Isolates of Staphylococcus aureus from Pakistan. Pathogens 10. 10.3390/pathogens10080918.
81. Ziebandt AK, Kusch H, Degner M, Jaglitz S, Sibbald MJ, Arends JP, Chlebowicz MA, Albrecht D, Pantucek R, Doskar J, et al. (2010). Proteomics uncovers extreme heterogeneity in the Staphylococcus aureus exoproteome due to genomic plasticity and variant gene regulation. Proteomics 10, 1634–1644. 10.1002/pmic.200900313. [PubMed: 20186749]
82. Meyer TC, Michalik S, Holtfreter S, Weiss S, Friedrich N, Völzke H, Kocher T, Kohler C, Schmidt F, Bröker BM, and Völker U (2021). A Comprehensive View on the Human Antibody Repertoire Against Staphylococcus aureus Antigens in the General Population. Front Immunol 12, 651619. 10.3389/fimmu.2021.651619. [PubMed: 33777051]
83. Radke EE, Brown SM, Pelzek AJ, Fulmer Y, Hernandez DN, Torres VJ, Thomsen IP, Chiang WK, Miller AO, Shopsin B, and Silverman GJ (2018). Hierarchy of human IgG recognition within the Staphylococcus aureus immunome. Sci Rep 8, 13296. 10.1038/s41598-018-31424-3. [PubMed: 30185867]
84. Nho Y, Lawson K, Banovic F, and Han L (2022). Staphylococcus aureus phenol-soluble modulins induce itch sensation. J Dermatol Sci 107, 48–51. 10.1016/j.jdermsci.2022.07.002. [PubMed: 35817662]

85. Bao C, Chen O, Sheng H, Zhang J, Luo Y, Hayes BW, Liang H, Liedtke W, Ji RR, and Abraham SN (2023). A mast cell-thermoregulatory neuron circuit axis regulates hypothermia in anaphylaxis. Sci Immunol 8, eadc9417. 10.1126/sciimmunol.adc9417. [PubMed: 36930731]
86. Stefansson K, Brattsand M, Roosterman D, Kempkes C, Bocheva G, Steinhoff M, and Egelrud T (2008). Activation of proteinase-activated receptor-2 by human kallikrein-related peptidases. J Invest Dermatol 128, 18–25. 10.1038/sj.jid.5700965. [PubMed: 17625593]
87. Frateschi S, Camerer E, Crisante G, Rieser S, Membrez M, Charles RP, Beermann F, Stehle JC, Breiden B, Sandhoff K, et al. (2011). PAR2 absence completely rescues inflammation and ichthyosis caused by altered CAP1/Prss8 expression in mouse skin. Nat Commun 2, 161. 10.1038/ncomms1162. [PubMed: 21245842]
88. Steinhoff M, Neisius U, Ikoma A, Fartasch M, Heyer G, Skov PS, Luger TA, and Schmelz M (2003). Proteinase-activated receptor-2 mediates itch: a novel pathway for pruritus in human skin. J Neurosci 23, 6176–6180. 10.1523/jneurosci.23-15-06176.2003. [PubMed: 12867500]
89. Williams MR, Nakatsuji T, Sanford JA, Vrbanac AF, and Gallo RL (2017). Staphylococcus aureus Induces Increased Serine Protease Activity in Keratinocytes. J Invest Dermatol 137, 377–384. 10.1016/j.jid.2016.10.008. [PubMed: 27765722]
90. Chua W, Poh SE, and Li H (2022). Secretory Proteases of the Human Skin Microbiome. Infect Immun 90, e0039721. 10.1128/iai.00397-21. [PubMed: 34606369]
91. Cau L, Williams MR, Butcher AM, Nakatsuji T, Kavanaugh JS, Cheng JY, Shafiq F, Higbee K, Hata TR, Horswill AR, and Gallo RL (2021). Staphylococcus epidermidis protease EcpA can be a deleterious component of the skin microbiome in atopic dermatitis. J Allergy Clin Immunol 147, 955–966.e916. 10.1016/j.jaci.2020.06.024. [PubMed: 32634452]
92. Lukomski S, Montgomery CA, Rurangirwa J, Geske RS, Barrish JP, Adams GJ, and Musser JM (1999). Extracellular cysteine protease produced by Streptococcus pyogenes participates in the pathogenesis of invasive skin infection and dissemination in mice. Infect Immun 67, 1779–1788. 10.1128/iai.67.4.1779-1788.1999. [PubMed: 10085018]
93. Baral P, Udit S, and Chiu IM (2019). Pain and immunity: implications for host defence. Nat Rev Immunol 19, 433–447. 10.1038/s41577-019-0147-2. [PubMed: 30874629]
94. Sorkin LS, Eddinger KA, Woller SA, and Yaksh TL (2018). Origins of antidromic activity in sensory afferent fibers and neurogenic inflammation. Semin Immunopathol 40, 237–247. 10.1007/s00281-017-0669-2. [PubMed: 29423889]
95. Chiu IM, von Hehn CA, and Woolf CJ (2012). Neurogenic inflammation and the peripheral nervous system in host defense and immunopathology. Nat Neurosci 15, 1063–1067. 10.1038/nn.3144. [PubMed: 22837035]
96. Souza-Moreira L, Campos-Salinas J, Caro M, and Gonzalez-Rey E (2011). Neuropeptides as pleiotropic modulators of the immune response. Neuroendocrinology 94, 89–100. 10.1159/000328636. [PubMed: 21734355]
97. de Garavilla L, Vergnolle N, Young SH, Ennes H, Steinhoff M, Ossovskaya VS, D'Andrea MR, Mayer EA, Wallace JL, Hollenberg MD, et al. (2001). Agonists of proteinase-activated receptor 1 induce plasma extravasation by a neurogenic mechanism. Br J Pharmacol 133, 975–987. 10.1038/sj.bjp.0704152. [PubMed: 11487506]
98. Ruhl CR, Pasko BL, Khan HS, Kindt LM, Stamm CE, Franco LH, Hsia CC, Zhou M, Davis CR, Qin T, et al. (2020). Mycobacterium tuberculosis Sulfolipid-1 Activates Nociceptive Neurons and Induces Cough. Cell 181, 293–305 e211. 10.1016/j.cell.2020.02.026. [PubMed: 32142653]
99. Bennett CF, Kordasiewicz HB, and Cleveland DW (2021). Antisense Drugs Make Sense for Neurological Diseases. Annu Rev Pharmacol Toxicol 61, 831–852. 10.1146/annurev-pharmtox-010919-023738. [PubMed: 33035446]
100. Halvorsen JA, Dalgard F, Thoresen M, Bjertness E, and Lien L (2012). Itch and pain in adolescents are associated with suicidal ideation: a population-based cross-sectional study. Acta Derm Venereol 92, 543–546. 10.2340/00015555-1251. [PubMed: 22068440]
101. Schneider G, Driesch G, Heuft G, Evers S, Luger TA, and Ständer S (2006). Psychosomatic cofactors and psychiatric comorbidity in patients with chronic itch. Clin Exp Dermatol 31, 762–767. 10.1111/j.1365-2230.2006.02211.x. [PubMed: 17040260]

102. Frey AM, Chaput D, and Shaw LN (2021). Insight into the human pathodegradome of the V8 protease from Staphylococcus aureus. Cell Rep 35, 108930. 10.1016/j.celrep.2021.108930. [PubMed: 33826899]

103. Motta JP, Denadai-Souza A, Sagnat D, Guiraud L, Edir A, Bonnart C, Sebbag M, Rousset P, Lapeyre A, Seguy C, et al. (2019). Active thrombin produced by the intestinal epithelium controls mucosal biofilms. Nat Commun 10, 3224. 10.1038/s41467-019-11140-w. [PubMed: 31324782]

104. Madisen L, Zwingman TA, Sunkin SM, Oh SW, Zariwala HA, Gu H, Ng LL, Palmiter RD, Hawrylycz MJ, Jones AR, et al. (2010). A robust and high-throughput Cre reporting and characterization system for the whole mouse brain. Nat Neurosci 13, 133–140. 10.1038/nn.2467. [PubMed: 20023653]

105. Hou B, Reizis B, and DeFranco AL (2008). Toll-like receptors activate innate and adaptive immunity by using dendritic cell-intrinsic and -extrinsic mechanisms. Immunity 29, 272–282. 10.1016/j.immuni.2008.05.016. [PubMed: 18656388]

106. Schmidlin F, Amadesi S, Dabbagh K, Lewis DE, Knott P, Bunnett NW, Gater PR, Geppetti P, Bertrand C, and Stevens ME (2002). Protease-activated receptor 2 mediates eosinophil infiltration and hyperreactivity in allergic inflammation of the airway. J Immunol 169, 5315–5321. 10.4049/jimmunol.169.9.5315. [PubMed: 12391252]

107. Boucher AA, Rosenfeldt L, Mureb D, Shafer J, Sharma BK, Lane A, Crowther RR, McKell MC, Whitt J, Alenghat T, et al. (2020). Cell type-specific mechanisms coupling protease-activated receptor-1 to infectious colitis pathogenesis. J Thromb Haemost 18, 91–103. 10.1111/jth.14641. [PubMed: 31539206]

108. Liu Q, Tang Z, Surdenikova L, Kim S, Patel KN, Kim A, Ru F, Guan Y, Weng HJ, Geng Y, et al. (2009). Sensory neuron-specific GPCR Mrgprs are itch receptors mediating chloroquine-induced pruritus. Cell 139, 1353–1365. 10.1016/j.cell.2009.11.034. [PubMed: 20004959]

109. Nassar MA, Stirling LC, Forlani G, Baker MD, Matthews EA, Dickenson AH, and Wood JN (2004). Nociceptor-specific gene deletion reveals a major role for Nav1.7 (PN1) in acute and inflammatory pain. Proc Natl Acad Sci U S A 101, 12706–12711. 10.1073/pnas.0404915101. [PubMed: 15314237]

110. Valtcheva MV, Copits BA, Davidson S, Sheahan TD, Pullen MY, McCall JG, Dikranian K, and Gereau R.W.t. (2016). Surgical extraction of human dorsal root ganglia from organ donors and preparation of primary sensory neuron cultures. Nat Protoc 11, 1877–1888. 10.1038/nprot.2016.111. [PubMed: 27606776]

111. Maurer K, Reyes-Robles T, Alonzo F 3rd, Durbin J, Torres VJ, and Cadwell K (2015). Autophagy mediates tolerance to Staphylococcus aureus alpha-toxin. Cell Host Microbe 17, 429–440. 10.1016/j.chom.2015.03.001. [PubMed: 25816775]

112. Joo HS, Cheung GY, and Otto M (2011). Antimicrobial activity of community-associated methicillin-resistant Staphylococcus aureus is caused by phenol-soluble modulin derivatives. J Biol Chem 286, 8933–8940. 10.1074/jbc.M111.221382. [PubMed: 21278255]

113. Austin CM, Garabaglu S, Krute CN, Ridder MJ, Seawell NA, Markiewicz MA, Boyd JM, and Bose JL (2019). Contribution of YjbIH to Virulence Factor Expression and Host Colonization in Staphylococcus aureus. Infect Immun 87. 10.1128/iai.00155-19.

114. Monk IR, Shah IM, Xu M, Tan MW, and Foster TJ (2012). Transforming the untransformable: application of direct transformation to manipulate genetically Staphylococcus aureus and Staphylococcus epidermidis. mBio 3. 10.1128/mBio.00277-11.

115. Luong TT, and Lee CY (2007). Improved single-copy integration vectors for Staphylococcus aureus. J Microbiol Methods 70, 186–190. 10.1016/j.mimet.2007.04.007. [PubMed: 17512993]

116. Crosby HA, Schlievert PM, Merriman JA, King JM, Salgado-Pabón W, and Horswill AR (2016). The Staphylococcus aureus Global Regulator MgrA Modulates Clumping and Virulence by Controlling Surface Protein Expression. PLoS Pathog 12, e1005604. 10.1371/journal.ppat.1005604. [PubMed: 27144398]

117. Mootz JM, Malone CL, Shaw LN, and Horswill AR (2013). Staphopains modulate Staphylococcus aureus biofilm integrity. Infect Immun 81, 3227–3238. 10.1128/iai.00377-13. [PubMed: 23798534]

118. Deng L, Schilcher K, Burcham LR, Kwiecinski JM, Johnson PM, Head SR, Heinrichs DE, Horswill AR, and Doran KS (2019). Identification of Key Determinants of Staphylococcus aureus Vaginal Colonization. mBio 10. 10.1128/mBio.02321-19.

119. VanDrisse CM, and Escalante-Semerena JC (2016). New high-cloning-efficiency vectors for complementation studies and recombinant protein overproduction in Escherichia coli and Salmonella enterica. Plasmid 86, 1–6. 10.1016/j.plasmid.2016.05.001. [PubMed: 27234933]

120. DuBreuil DM, Chiang BM, Zhu K, Lai X, Flynn P, Sapir Y, and Wainger BJ (2021). A high-content platform for physiological profiling and unbiased classification of individual neurons. Cell Rep Methods 1. 10.1016/j.crmeth.2021.100004.

121. Yousuf MS, Samtleben S, Lamothe SM, Friedman TN, Catuneanu A, Thorburn K, Desai M, Tenorio G, Schenk GJ, Ballanyi K, et al. (2020). Endoplasmic reticulum stress in the dorsal root ganglia regulates large-conductance potassium channels and contributes to pain in a model of multiple sclerosis. Faseb j 34, 12577–12598. 10.1096/fj.202001163R. [PubMed: 32677089]

122. Voisin T, Perner C, Messou MA, Shiers S, Ualiyeva S, Kanaoka Y, Price TJ, Sokol CL, Bankova LG, Austen KF, and Chiu IM (2021). The CysLT(2)R receptor mediates leukotriene C(4)-driven acute and chronic itch. Proc Natl Acad Sci U S A 118. 10.1073/pnas.2022087118.

123. Mihara K, Ramachandran R, Renaux B, Saifeddine M, and Hollenberg MD (2013). Neutrophil elastase and proteinase-3 trigger G protein-biased signaling through proteinase-activated receptor-1 (PAR1). J Biol Chem 288 , 32979–32990. 10.1074/jbc.M113.483123. [PubMed: 24052258]

HIGHLIGHTS

- *S. aureus* induces itch and scratch damage with epicutaneous skin exposure
- V8 protease (SspA) is necessary and sufficient for itch during *S. aureus* exposure
- *S. aureus* V8 activates mouse and human sensory neurons through PAR1
- PAR1 deficiency or blockade abrogates *S. aureus* induced itch and skin damage

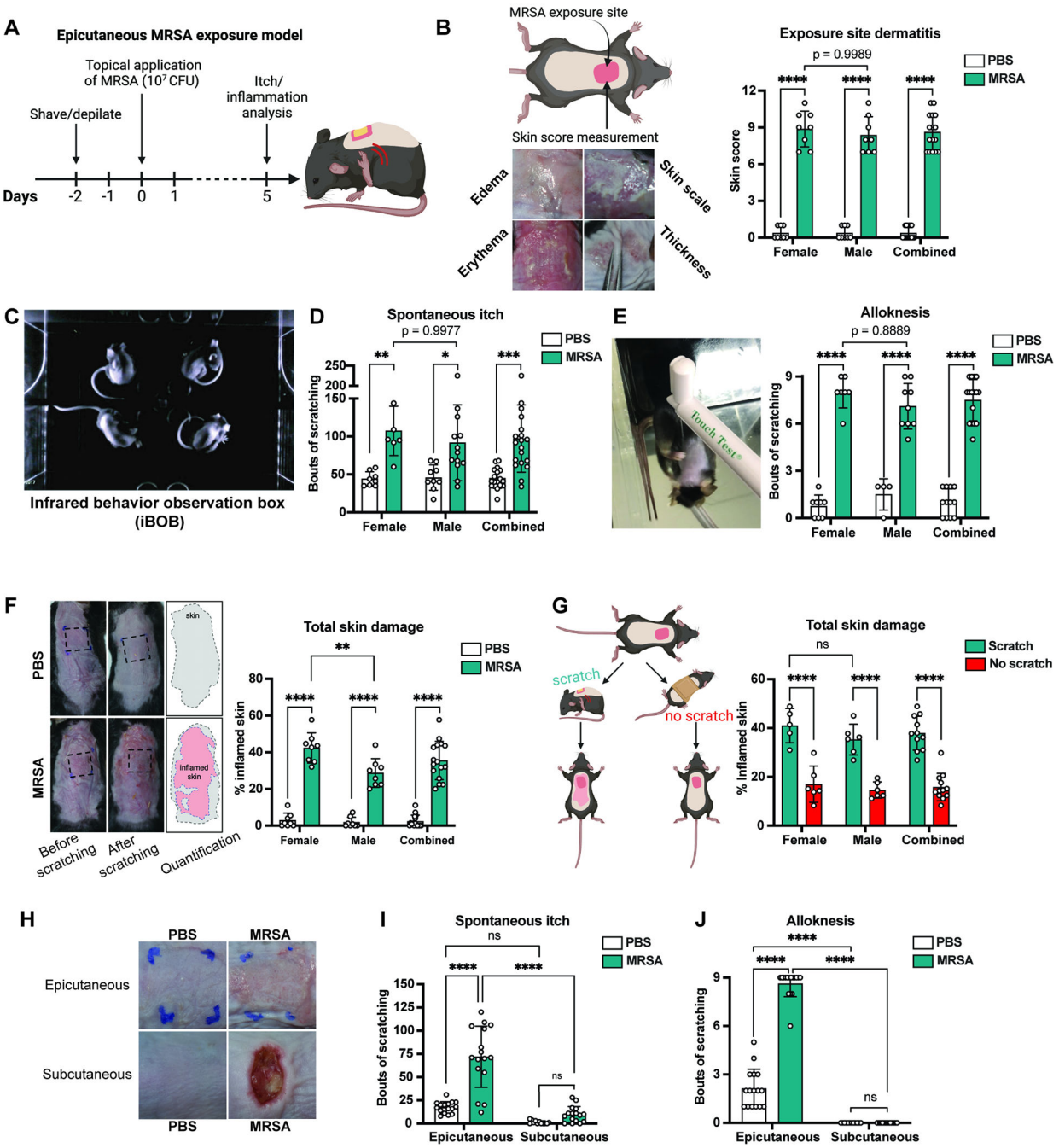

Figure 1. Epicutaneous *S. aureus* induces itch and scratch-induced skin pathology.

(A) Murine model of *S. aureus* exposure and itch analysis

(B-E) 5-days after epicutaneous exposure, dermatitis (B), spontaneous itch (C-D), and (E) alloknesis were measured (n=8-13 males, 6-8 females per group)

(F) Analysis of total skin damage after scratching (n=8 males, 8 females per group)

(G) Total skin damage in mice allowed to scratch or prevented from scratching (n=6 males, 5-6 females per group)

(H-J) Mice inoculated with *S. aureus* epicutaneously or infected subcutaneously; Representative images (H), spontaneous itch (I), and alloknesis (J) on day-5 (n=16 per group)

For each panel, data combined from 2 independent experiments are shown. Data are represented as mean±SD.

Statistical analysis: (B, D, E, F, G, I, J) Two-way ANOVA with Sidak's multiple comparisons. *P<0.05; **P<0.01; ***P<0.001; ****P<0.0001; ns, not significant. See also Figure S1, S2, and S3.

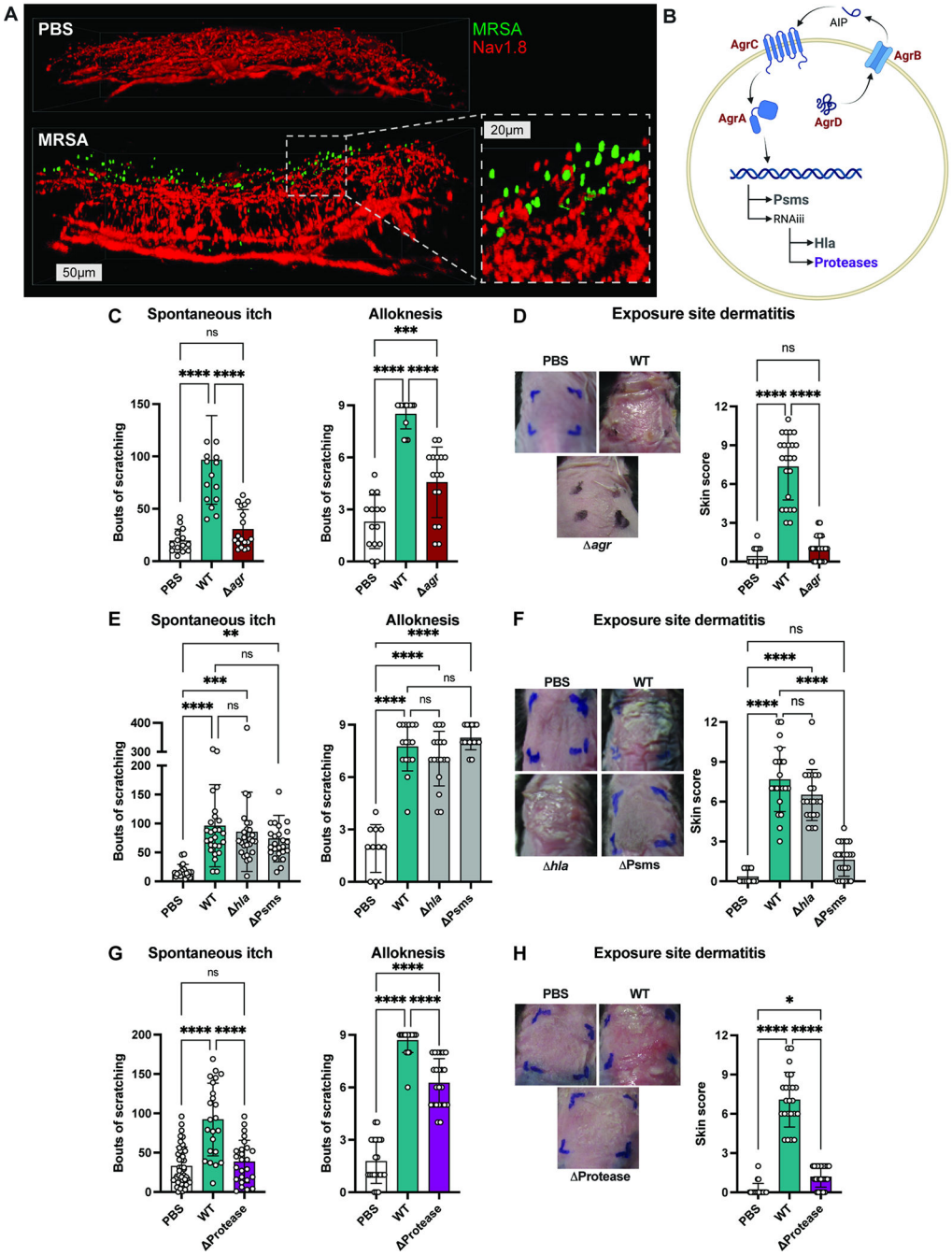

Figure 2. Bacterial factors including Agr quorum sensing and proteases mediate itch.

(A) Whole mount images of skin from Nav1.8-tdTomato mice treated with PBS or GFP-MRSA (scale bars, 50 or 20μm)

(B) Agr quorum sensing regulates expression of phenol soluble modulins (Psms), alpha-toxin (Hla), and proteases

(C-D) Spontaneous itch, alloknesis (C) and dermatitis scores (D) recorded for control mice (PBS) or mice inoculated with WT or Δ*agr* MRSA (n=10 males, 10 females per group)

(E-F) Spontaneous itch, alloknesis (E) and dermatitis scores (F) for control mice (PBS) or mice inoculated with WT, Δ*hla* or ΔPsms MRSA (n=8-15 males, 8-16 females per group)
(G-H) Spontaneous itch, alloknesis (G) and dermatitis scores (H) for control mice (PBS) or mice inoculated with WT or ΔProtease MRSA (n=12 males, 12 females per group).
For each panel, data combined from 4-6 independent experiments are shown. Data are represented as mean±SD.
Statistical analysis: (C-H) One-way ANOVA. *P<0.05; **P<0.01; ***P<0.001; ****P<0.0001; ns, not significant. See also Figure S4 and Table S1.

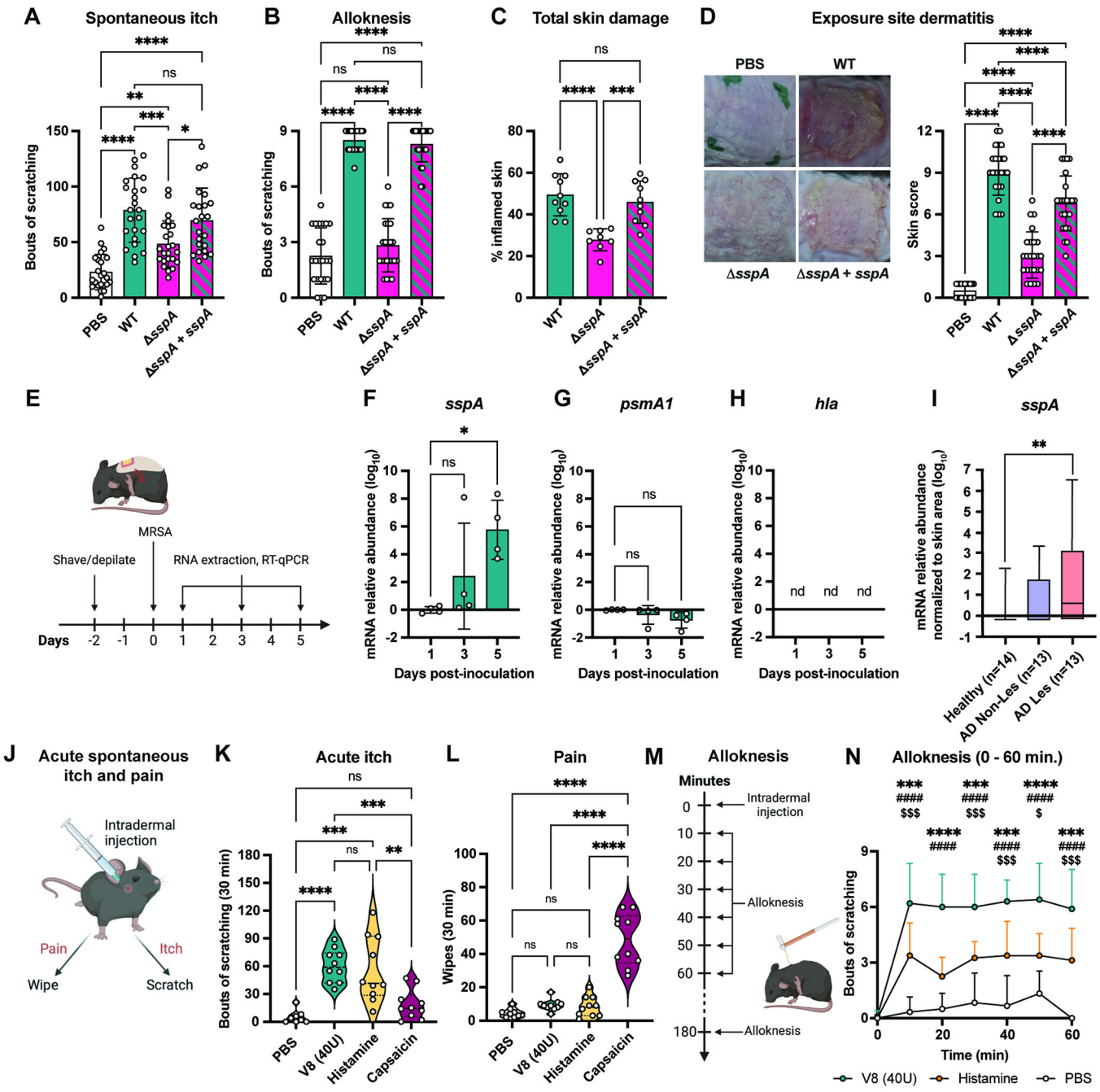

Figure 3. *S. aureus* V8 protease contributes to itch and inflammation.

(A-B) Spontaneous itch (A) and alloknesis (B) for control mice (PBS) or mice inoculated with WT, Δ*sspA*, or Δ*sspA + sspA* MRSA (n=11-12 males, 12 females per group)

(C) Total skin damage for control (PBS) or mice inoculated with WT, Δ*sspA*, or Δ*sspA + sspA* MRSA (n=4-5 males, 4-5 females per group)

(D) Representative skin images and dermatitis scores from control mice (PBS) or mice inoculated with WT, Δ*sspA*, or Δ*sspA + sspA* MRSA (n= 11-12 males, 12 females per group)

(E-H) Skin collected from mice at 1-, 3-, and 5-days post-inoculation with MRSA quantified for *sspA* (F), *psmA1* (G), and *hla* (H) transcripts (normalized to 1-day post-inoculation) (n=2 males, 2 females per group)

(I) Quantification of *sspA* mRNA from skin swabs from healthy human subjects or non-lesional and lesional skin from AD patients (n=13-14 per group)

(J) Mouse acute itch and pain behavior

(K-L) Acute itch (K) and pain (L) following intradermal injection with PBS, V8, histamine or capsaicin (n=4-5 males, 4-5 females per group)

(M) Mouse intradermal injection and alloknesis model

(N) Alloknesis after injection with PBS, V8, or histamine (n=3-5 males, 3-5 females per group) For each panel, data combined from 2 independent experiments are shown. Data are represented as mean±SD.

Statistical analysis: (A-D, F-I, K-L) One-way ANOVA. (N) Two-way ANOVA, Tukey's multiple comparisons. *V8 vs. Histamine; #Histamine vs. PBS; $V8 vs. PBS; *P<0.05; **P<0.01; ***P<0.001; ****P<0.0001; ns, not significant. See also Figure S5.

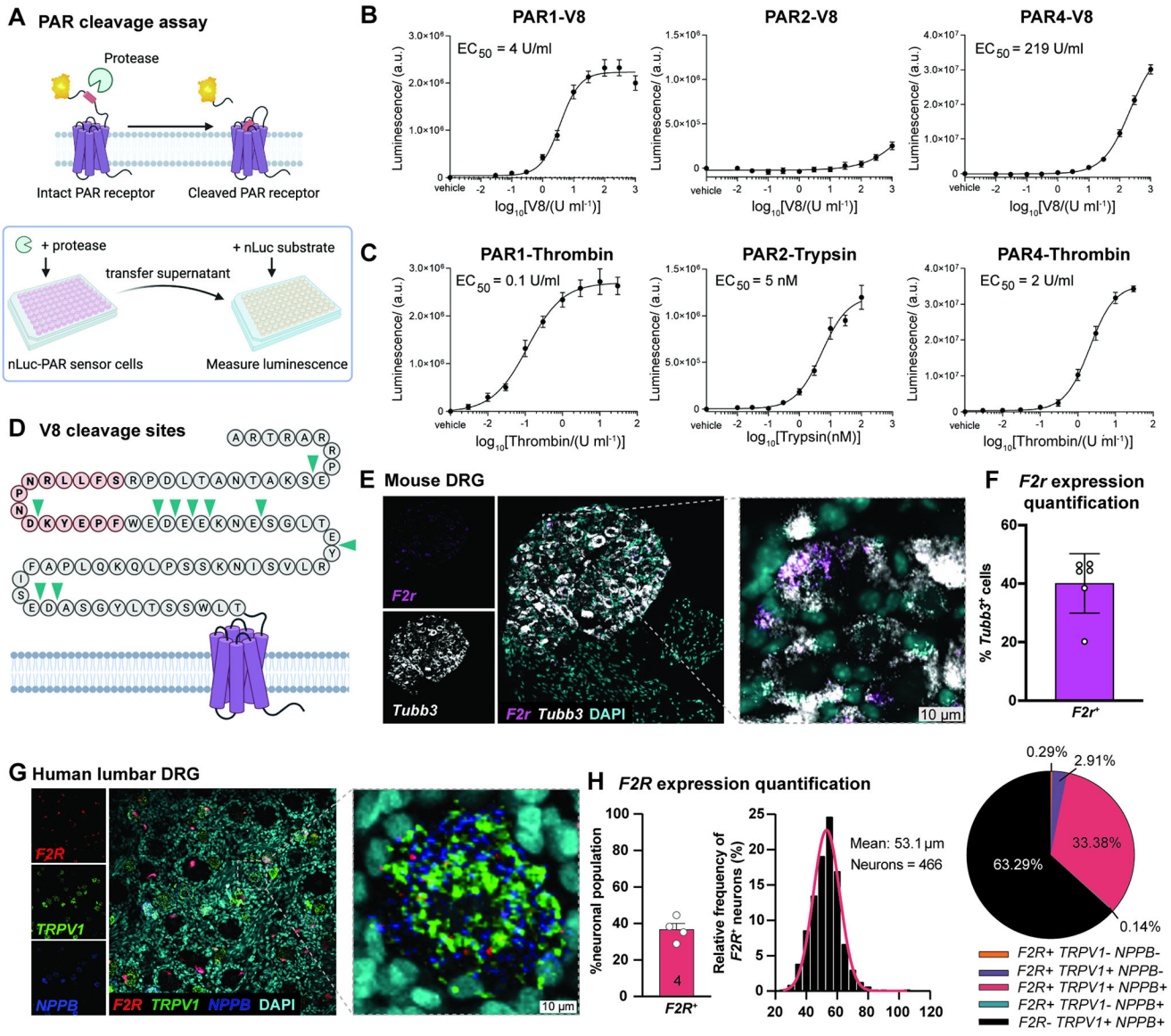

Figure 4. V8 protease cleaves PAR1, which is expressed by pruriceptors

(A) PAR cleavage assays using nLuc-PAR-eYFP-CHO cells

(B-C) Cleavage data of human PAR1, 2, 4 by V8 protease, or thrombin (for PAR1, PAR4) or trypsin (for PAR2).

(D) V8 cleavage sites (arrows) on N-terminus of human PAR1 identified by mass spectrometry

(E) Representative images of RNAscope hybridization of mouse DRG sections for *F2r* and *Tubb3*

(F) Quantification of *F2r* expression in *Tubb3*-positive mouse neurons averaged per mouse (n=3 males, 3 females). Data are represented as mean±SD.

(G) Representative images of RNAscope hybridization of human DRG sections for *F2R, TRPV1,* and *NPPB*. Total of 1,328 neurons analyzed across 4 donors.

(H) Quantification of *F2R* expression in human neurons, proportions and frequency by size and marker expression. See also Figure S6 and Table S2.

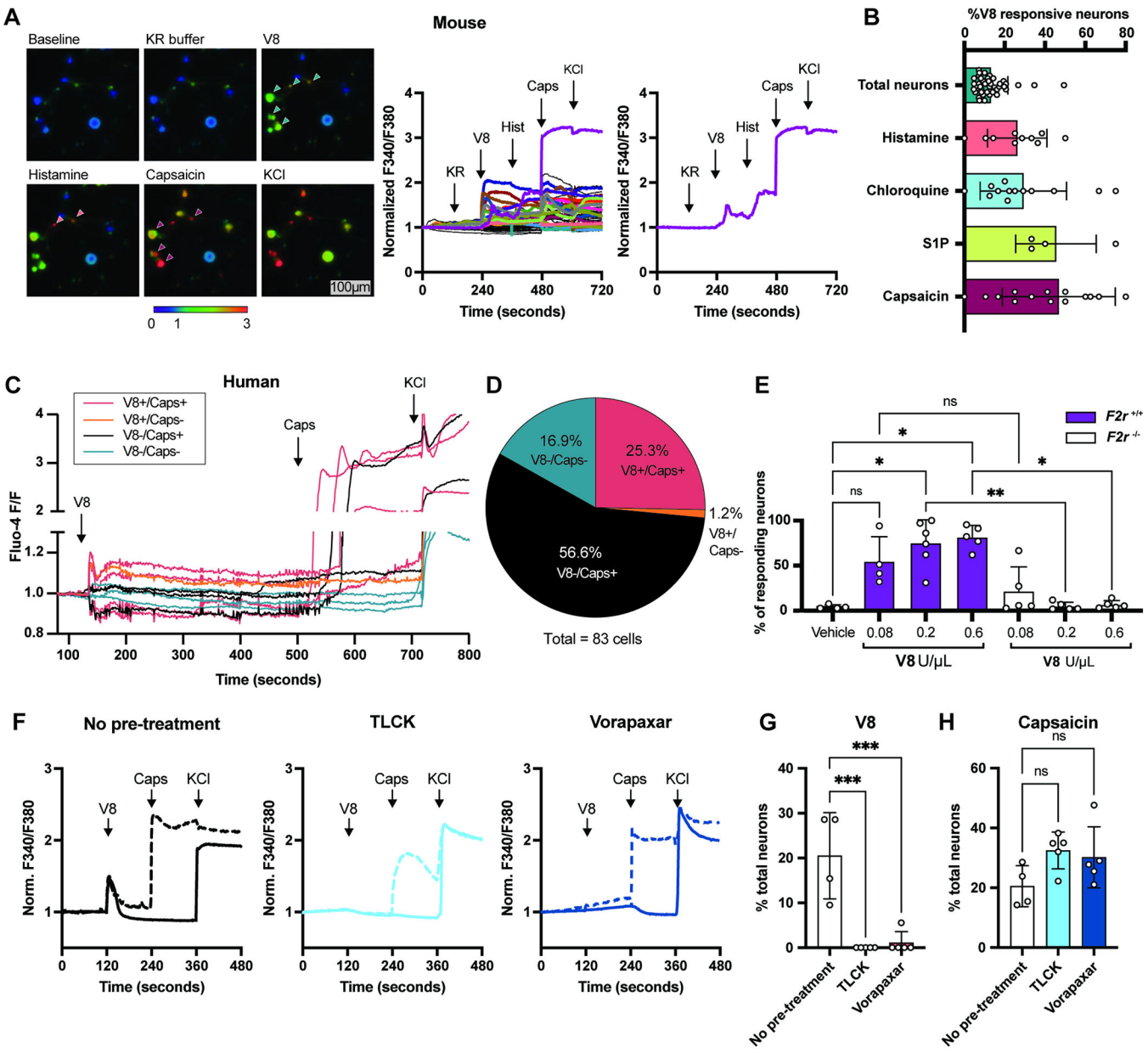

Figure 5. V8 protease directly activates pruriceptor neurons

(A) Representative Fura-2 ratiometric fields and calcium traces of mouse DRG neurons. Scale, 100μm.

(B) Percentages of total neurons (responsive to KCl) (n=41 fields) histamine-responsive (n= 10 fields) chloroquine-responsive (n=14 fields), S1P-responsive (n=4 fields) and capsaicin-responsive (n=16 fields) neurons that also respond to V8.

(C) Calcium traces of human DRG neurons from a representative dish treated with V8, capsaicin, KCl

(D) Pie chart showing human neuron populations responding to V8 and capsaicin (V8+/Cap+), V8 alone (V8+/Cap−), capsaicin alone (V8−/Cap+), and unresponsive to either (V8−/Cap−)

(E) Calcium imaging analysis of DRG neurons from *F2r*$^{+/+}$ and *F2r*$^{-/-}$ mice treated with increasing doses of V8

(F) Representative calcium traces of DRG neurons treated with V8, capsaicin, KCl with no pre-treatment (left) or 5 min. post-treatment with TLCK (middle) or Vorapaxar (right).

(G-H) Percentage of untreated neurons and neurons pre-treated with TLCK or Vorapaxar responding to V8 (G) or capsaicin (H).

For each panel, data combined from 5 independent experiments are shown. Data are represented as mean±SD.

Statistical analysis: (B, E, G, H) One-way ANOVA. *P<0.05; **P<0.01; ***P<0.001; ns, not significant. See also Figure S7.

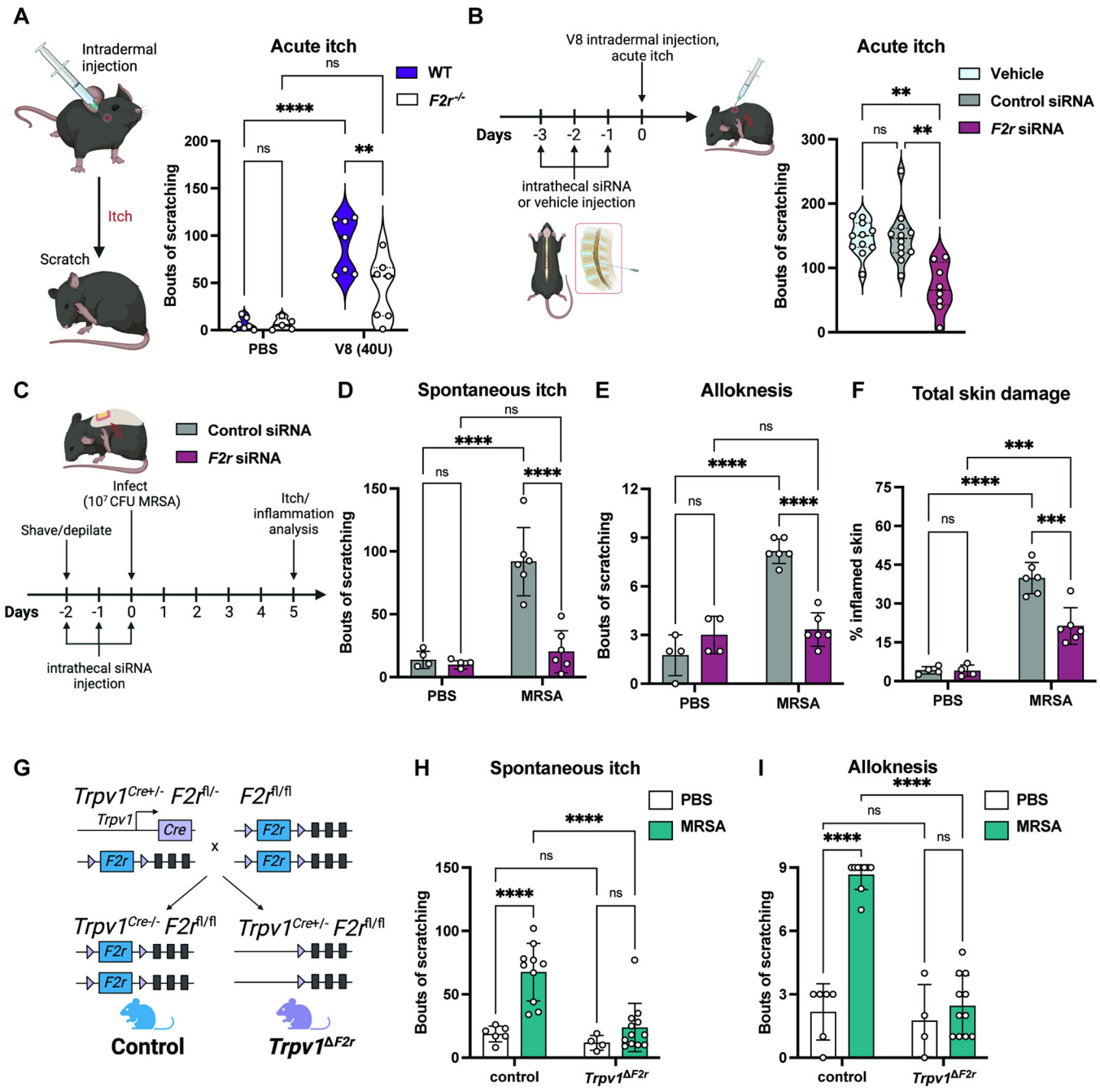

Figure 6. Neuronal PAR1 (*F2r*) is required for V8 and *S. aureus*-induced itch

(A) PBS or V8 protease injected intradermally into cheek of wildtype ($F2r^{+/+}$) and $F2r^{-/-}$ mice, spontaneous scratching over 30 min. (n=3-4 males, 2-4 females per group)

(B) Acute itch behaviors measured for mice treated with vehicle, control siRNA, or *F2r* siRNA (n=4-6 males, 4-6 females per group).

(C-F) Mice receiving intrathecal siRNA injections were treated with PBS or exposed to MRSA. Spontaneous itch (D), alloknesis, (E) and scratch-induced skin damage (F) measured 5-days post-exposure (n=4-6 males per group).

(G) Generation of *Trpv1*$^{\Delta F2r}$ and *Trpv1*$^{cre-}$ control mice.
(H-I) Spontaneous itch (H) and alloknesis (I) for *Trpv1*$^{\Delta F2r}$ and control mice treated with PBS or exposed to MRSA (n=3-8 males, 1-6 females per group).
For each panel, data combined from 2-3 independent experiments are shown. Data are represented as mean±SD.
Statistical analysis: (A, D-F, H, I) Two-way ANOVA, Sidak's multiple comparisons. (B, E) Mann-Whitney test. **P<0.01; ***P<0.001; ****P<0.0001; ns, not significant. See also Figure S8.

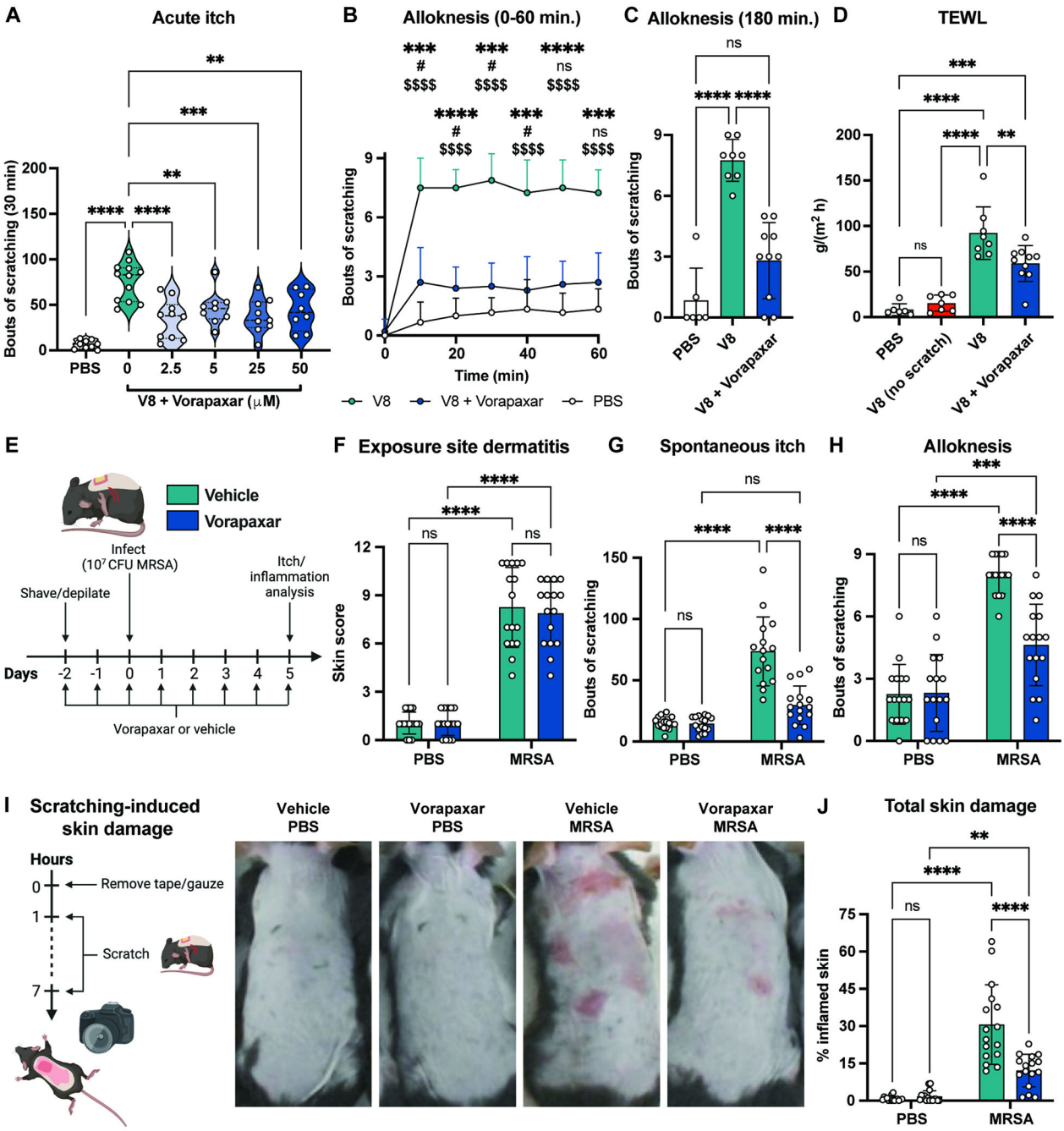

Figure 7. Treatment with PAR1 antagonist reduces itch and skin damage during *S. aureus* exposure

(A) Bouts of scratching following cheek injection with PBS or V8 with increasing doses of Vorapaxar (n=4-6 males, 4-6 females per group).

(B-C) Alloknesis measured every 10 min. for 1hr (B) and 3 hrs (C) after cheek injection with PBS, V8, or V8+Vorapaxar (n=3-5 males, 3-5 females per group).

(D) Mice injected with PBS, V8, or V8+Vorapaxar were allowed to scratch; TEWL measured 3 hrs post-injection. One group of V8-injected mice were wrapped in bandages to prevent scratching.

(E-J) Mice gavaged daily with vehicle or Vorapaxar from 2-days before exposure to PBS or MRSA. Dermatitis scores (F), spontaneous itch (G), alloknesis (H), scratch-induced skin damage (I-J) measured for control and MRSA-exposed mice treated with vehicle or Vorapaxar (n=7-8 males, 8 females per group)

For each panel, data combined from 2 independent experiments are shown. Data are represented as mean±SD.

Statistical analysis: (A, C, D) Mann-Whitney test (B) Two-way ANOVA with Tukey's multiple comparisons: *V8 vs. V8+Vorapaxar; #V8+Vorapaxar vs. PBS; $V8 vs. PBS (F-H, J) Two-way ANOVA with Sidak's multiple comparisons. *P<0.05; **P<0.01; ***P<0.001; ****P<0.0001; ns, not significant. See also Figure S9.

Key resources table

REAGENT or RESOURCE	SOURCE	IDENTIFIER
Antibodies		
eBioscience™ Fixable Viability Dye eFluor™506	Thermo Fisher	Cat. # 65-0866-18
Alexa Fluor® 700 anti-mouse CD45 Antibody	Biolegend	Cat. # 103128
APC anti-mouse CD45 Antibody	Thermo Fisher	Cat. # 17-0451-82
CD11c Monoclonal Antibody, Biotin	Thermo Fisher	Cat. # 13-0114-85
F4/80 Monoclonal Antibody, FITC	Thermo Fisher	Cat. # 11-4801-82
Ly-6G/Ly-6C Monoclonal Antibody, FITC	Biolegend	Cat. # 108406
CD3 Monoclonal Antibody, PerCP-eFluor 710	Thermo Fisher	Cat. # 46-0032-82
CD117 (c-Kit) Monoclonal Antibody, APC	Thermo Fisher	Cat. #17-1172-83
BV421 Rat Anti-Mouse IgE	BD Biosciences	Cat. # 564207
Brilliant Violet 605™ anti-mouse CD4 Antibody	Biolegend	Cat. # 100548
APC/Cyanine7 anti-mouse CD8a Antibody	Biolegend	Cat. # 100714
PE-CF594 Rat Anti-Mouse Siglec-F	BD Biosciences	Cat. # 562757
TCR gamma/delta Monoclonal Antibody, PE	Thermo Fisher	Cat. # 12-5711-82
PE/Cyanine7 anti-mouse/human CD11b	Biolegend	Cat. # 101216
SAV-BV605	Biolegend	Cat. # 405229
Bacterial and virus strains		
Staphylococcus aureus CA-MRSA LAC/USA300	Chiu et. al (2013)[12]	N/A
GFP-MRSA	Chiu et. al (2013)[12]	N/A
MRSA Δ*agr*	Maurer et al. (2015)[110]	N/A
MRSA Δ*hla*	Maurer et al. (2015)[110]	N/A
MRSA ΔPsms (Δ*psmα* Δ*psmβ* Δ*hld*)	Joo et al. (2011)[111]	N/A
MRSA ΔProteases (Δ*aur* Δ*scpA* Δ*sspAB spl::erm*)	Austin et al. (2019)[112]	N/A
MRSA Δ*aur*	Austin et al. (2019)[112]	N/A
MRSA Δ*scpA* Δ*sspB*	Austin et al. (2019)[112]	N/A
MRSA *spl::erm*	Austin et al. (2019)[112]	N/A
MRSA Δ*sspA*	This study	N/A
MRSA Δ*sspA + sspA*	This study	N/A
E. coli BL21 (Novagen)	EMD Millipore	Cat. # 70235-3
Biological samples		
Human dorsal root ganglia	Southwest Transplant Alliance	N/A
Human skin swabs	University of California San Diego	Cau et al. (2021)[90]
Chemicals, peptides, and recombinant proteins		
Tryptic Soy Agar	BD Difco	Cat. #236920
Tryptic Soy Broth	Sigma	Cat. #T8907
CHROMagar Staph aureus	Hardy Diagnostics	Cat. #G311
Cefoxotin	Cayman Chemical Company	Cat. #15990

REAGENT or RESOURCE	SOURCE	IDENTIFIER
Terrific Broth	BD Difco	Cat. # BD 243820
Ampicillin	Sigma	Cat. #A9518
Chloramphenicol	Sigma	Cat. #C0857
Isopropyl β-D-1-thiogalactopyranoside	Sigma	Cat. #I6758
RNA Protect Bacteria Reagent	Qiagen	Cat. #76506
Beta-mercaptoethanol	Sigma	Cat. #63689
V8 protease	Worthington	Cat. #LS003605
Histamine	Sigma	Cat. #H7125
Capsaicin	Tocris	Cat. #0462
Sphingosine-1-phosphate	Tocris	Cat. #1370
Vorapaxar	Axon Med Chem	Cat. #17555
SCH79797 dihydrochloride	Tocris	Cat. #1592
BMS 986120	Cayman Chemicals	Cat. #23497
Keratinocyte serum-free medium	Gibco	Cat. #17005-042
Keratinocytes supplements	Gibco	Cat. #37000-015
Human recombinant epidermal growth factor	BD	Cat. #354052
Pierce Ni-NTA Magnetic Agarose Beads	Thermo Fisher	Cat. #78605
Collagenase A	Sigma	Cat. #10103586001
Dispase II	Sigma	Cat. #D4693
Neuralbasal^{Tm} Medium	Thermo Fisher	Cat. #21103049
B27 serum-free supplement	Invitrogen	Cat. #17504-044
L-Glutamine	Invitrogen	Cat. #25-030-081
Pen/Strep	Thermo Fisher	Cat. #15140122
Nerve growth factor	Invitrogen	Cat. #50385-MNAC-250
Fura-2-AM	Life Technologies	Cat. #F-1221
STEMxyme I	Worthington	Cat. #LS004106
DNAse I	Worthington	Cat. #LS002139
BrainPhys media	STEMCell	Cat. #0752
SM1	STEMCell	Cat. #05711
GlutaMax	Thermo Fisher	Cat. #35050061
Fluo-4-AM	Thermo Fisher	Cat. #F14201
Pluronic F-127	Thermo Fisher	Cat. #P3000MP
Ham's F-12	Gibco	Cat. #11765054
Fetal bovine Serum	R&D Systems	Cat. #S11150H
Geneticin$^{™}$ selective antibiotic	Thermo Fisher	Cat. #10131035
DMEM	Gibco	Cat. #10313039
In Vivo JetPEI	Polyplus Transfection	Cat. #101000040
Critical commercial assays		
Pierce BCA Protein Assay	ThermoFisher	Cat. #23227

REAGENT or RESOURCE	SOURCE	IDENTIFIER
Direct-zol RNA MiniPrep Plus kit	Zymo Research	Cat. #R2071
iScript cDNA synthesis kit	Bio-Rad	Cat. #1708891
RNAscope Probe-Mm-F2r	Advanced Cell Diagnostics	Cat. #438511
RNAscope Probe-Mm-Tubb3-C2	Advanced Cell Diagnostics	Cat. #423391-C2
RNAscope Multiplex V2 kit	Advanced Cell Diagnostics	Cat. #323110
RNAscope Probe-Hs-F2R-C2	Advanced Cell Diagnostics	Cat. #471081-C2
RNAscope Probe-HS-TRPV1-C3	Advanced Cell Diagnostics	Cat. #415381-C3
RNAscope Probe-Hs-NPPB-C1	Advanced Cell Diagnostics	Cat. #448511
NucleoSpin RNA isolation kit	Macherey-Nagel	Cat. #740955.50
Deposited data		
Mouse nervous system transcriptomic data http://mousebrain.org/	Zeisel et al. (2018)[61]	NCBI SRA repository (SRP135960)
Human dorsal root ganglia transcriptomic data http://sensoryomics.com/	Taveres-Ferreira et al. (2022)[65]	dbGaP repository (phs001158)
Experimental models: Cell lines		
KERTr immortalized human keratinocytes	ATCC	CRL-2309
CHO-K1	ATCC	CCL-61
HEK-293	ATCC	CFL-1573
Experimental models: Organisms/strains		
C57/BL6NTac (Opportunist Free)	Taconic Biosciences	Strain #B6
C57/BL6J	JAX	Strain #000664
B6.Rosa26-stop(flox)- tdTomato	JAX	Strain #007914
B6.129P2(SJL)-*Myd88*$^{tm1.1Defr}$/J	JAX	Strain #009088
B6.Cg-*F2rl1*^{tm1Mslb}/J	JAX	Strain #004993
B6.Cg-*Kit*$^{W\text{-}sh}$	JAX	Strain #030764
B6.129-*Trpv1*$^{tm1(cre)Bbm}$/J strain	JAX	Strain #0017769
C57BL/6NTac.Cg-*Rag2*^{tm1Fwa} *Il2rg*^{tm1Wjl}	Taconic Biosciences	Strain #4111
F2r-flox	Boucher et al. (2020)[106]	N/A
Balbc/J	JAX	Strain #00651
BALB/c-*Il4ra*^{tm1Sz}/J	JAX	Strain #003514
Mrgpr knockout	Liu et al. (2009)[107]	N/A
Nav1.8-Cre	Nassar et al. (2004)[108]	N/A
B6.129S4-*F2r*^{tm1Ajc}/J	JAX	Strain #002862
Oligonucleotides		
sspA-F: ACCTGTAGCAACAATGTGGGA	Synthesized by Thermo Fisher	N/A
sspA-R: ATTTGGTACACCGCCCCAAT	Synthesized by Thermo Fisher	N/A
psmA1-F: GTATCATCGCTGGCATCA	Synthesized by Thermo Fisher	N/A
psmA1-R: AAGACCTCCTTTGTTTGTTATG	Synthesized by Thermo Fisher	N/A
hla-F: AGCAGCAGATAACTTCCT	Synthesized by Thermo Fisher	N/A
hla-R: TGGTAGTCATCACGAACT	Synthesized by Thermo Fisher	N/A

REAGENT or RESOURCE	SOURCE	IDENTIFIER
il31ra-F: CCCTGTGTTGTCCTGATGTTCCCA	Synthesized by Thermo Fisher	N/A
il31ra-R: ACCCTTTCCAGCTTCCTCTGTCAA	Synthesized by Thermo Fisher	N/A
f2r-F: CCTATGAGCGAGCCAGAATC	Synthesized by Thermo Fisher	N/A
f2r-R: TAGACTGCCCTACCCTCCAG	Synthesized by Thermo Fisher	N/A
Recombinant DNA		
Plasmid pLL29erm	Luong et al. (2007)[114] Crosby et al. (2016)[115]	N/A
Software and algorithms		
FlowJo™ Software version 10.2	BD Life Sciences	www.flowjo.com
Graphpad Prism version 9.5.1	Graphpad	www.graphpad.com
LAS X Life Science Microscope Software	Leica	
Other		
Stellaris 8 FALCON CFS confocal microscope	Leica	N/A
QuantStudio Real-Time PCR Instrument	Thermo Fisher	N/A
CFX96 Real-Time Detection System	Bio-Rad	N/A
LSR Fortessa flow cytometer	BD Biosciences	N/A
Eclipse Ti inverted microscope	Nikon	N/A
Zyla sCMOS camera	Andor	N/A